THESIS

COMPUTATIONAL FLUID DYNAMICS (CFD) MODELING FOR CdTe SOLAR CELL MANUFACTURING

Submitted by

Kevin Eugene Walters

Department of Mechanical Engineering

In partial fulfillment of the requirements

For the Degree of Master of Science

Colorado State University

Fort Collins, Colorado

Fall 2011

Master's Committee:

Advisor: Walajabad Sampath
Co-Advisor: Hiroshi Sakurai

James Sites

ABSTRACT

COMPUTATIONAL FLUID DYNAMICS (CFD) MODELING FOR CdTe SOLAR CELL MANUFACTURING

The CdTe solar cell manufacturing process developed at Colorado State University used a vapor source that utilized infrared heating lamps as the heating source. This was used in the initial research system that was used to develop the inline CdTe solar cell manufacturing method used in industry. This system has since been redesigned to improve its ability to function as a more versatile research tool.

This thesis focuses on the modeling efforts used in the development and understanding of an embedded NiCr heating unit for the vapor source. The traditional infrared heating lamps, while effective, were inefficient. A new design consisting of a NiCr heating element imbedded in to the graphite deposition crucible, was developed as a more efficient and robust replacement to the infrared lamps. Four distinct models of increasing complexity were developed using the heat transfer modeling capabilities of ANSYS Fluent. The first two models helped to determine the overall thermal uniformity and the ability of the new heating designs ability to reach the needed temperatures of the deposition processes.

The third model discussed in this thesis, aided in the development of the top heater that would maintain the desired steady state temperature at the process station used to deposit CdS films. The final model developed contains a higher level of detail used to determine the validity of previous assumptions and to gain an understanding of the internal temperature profile of the completed source.

This modeling effort was extended to the system used in industry. The experimental data was compared to the modeled data verifying the model accuracy. The calculated temperatures were within 2.5% of the measured temperatures. The modeling efforts of both the CSU and Abound Solar deposition systems have proved the usefulness of CFD modeling as an important tool to equipment development and characterization.

ACKNOWLEDGEMENTS

I would like to thank my advisor, Professor Sampath for bringing me into his laboratory. Without his support and drive to make computer modeling an important part of engineering design, this project would not have progressed. I would also like to give thanks to my co-advisor Professor Hiroshi Sakurai. He has been vital to my understanding of CFD modeling technique. Additionally I would like to give thanks to my committee member Professor Jim Sites for his continued support of the modeling effort within the I/UCRC (Industry/University Cooperative Research Center) and the subsequent projects for Abound Solar.

I thank Dennis Csehi, Warren Salt, and Jeff Wicks from Abound Solar for interest in expanding the modeling capabilities at Abound Solar. Without their help I would not have had access to create, run and evaluate large industrial sized systems.

I also need to extend my appreciation out to the National Science foundation for supporting the creation of the I/UCRC at CSU. The IAB (Industrial Advisory Board) member of the I/UCRC for their support of the modeling project. All of the members of the Materials engineering laboratory involved with the creation of the ARDS (Advanced Research Deposition System); Jason Kephart, Pual Kobyakov.

I need to give special thanks to Nicole Landau for her initial work on the embedded heater concept.

Finally, to my family who have been there to support my late nights and weekends. Without them I would not have had the time to complete this achievement.

TABLE OF CONTENTS

TABLE OF FIGURES

Chapter 1: Introduction

1.1 Energy, Environment, and Humanity.

Since Thomas Edison made the light bulb practical, the Wright brothers began to fly, and the automobile became a primary form of transportation, the need for, and consumption of energy has increased at an insurmountable rate. In addition to increased demand for energy, we face serious global climate change caused by the increased concentration of greenhouse gasses. Greenhouse gas concentrations have increased 70% since 1970 as a result of human activities Figure 1[1(p5)]. The increase in greenhouse gas concentrations has paralleled our increase in energy consumption. This is due to the fact that the primary source of energy has been fossil fuels Figure 2[2(p37)]. The world energy consumption continues to be on the rise with a predicted 50% increase by 2035 Figure 3[3]. The world needs to find alternative forms of energy to sustain this growth while reducing our greenhouse gas emissions.

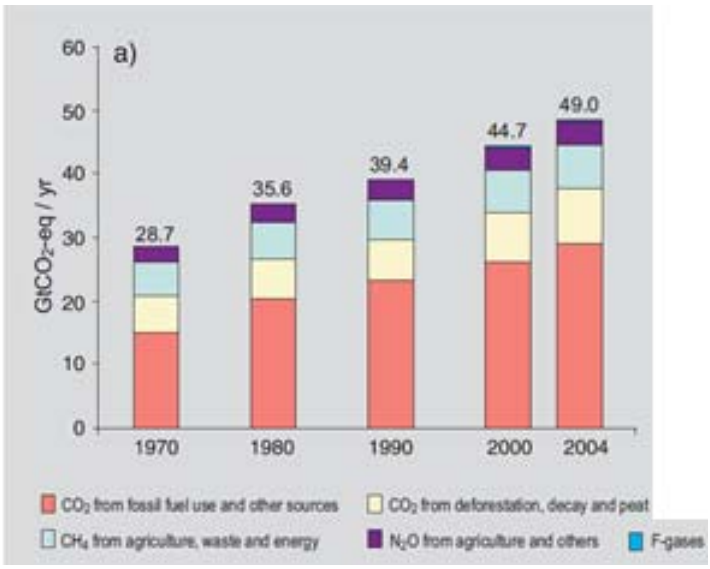

Figure 1:(a) Global Annual Emissions of Anthropogenic GHGs from 1970 to 2004(CO_2 Only). [1(p5)]

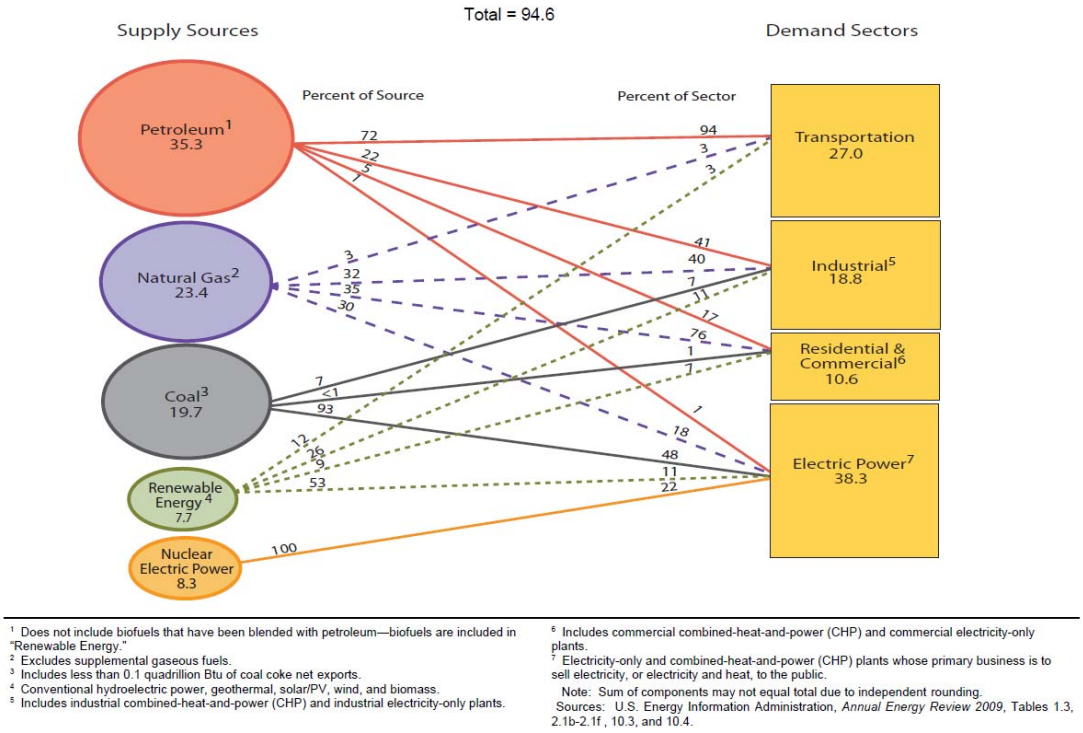

[1] Does not include biofuels that have been blended with petroleum—biofuels are included in "Renewable Energy."
[2] Excludes supplemental gaseous fuels.
[3] Includes less than 0.1 quadrillion Btu of coal coke net exports.
[4] Conventional hydroelectric power, geothermal, solar/PV, wind, and biomass.
[5] Includes industrial combined-heat-and-power (CHP) and industrial electricity-only plants.
[6] Includes commercial combined-heat-and-power (CHP) and commercial electricity-only plants.
[7] Electricity-only and combined-heat-and-power (CHP) plants whose primary business is to sell electricity, or electricity and heat, to the public.

Note: Sum of components may not equal total due to independent rounding.
Sources: U.S. Energy Information Administration, *Annual Energy Review 2009*, Tables 1.3, 2.1b-2.1f , 10.3, and 10.4.

Figure 2: Primary Energy Flow by Source and Sector, 2009 - U.S. Energy Information Administration / Annual review 2009

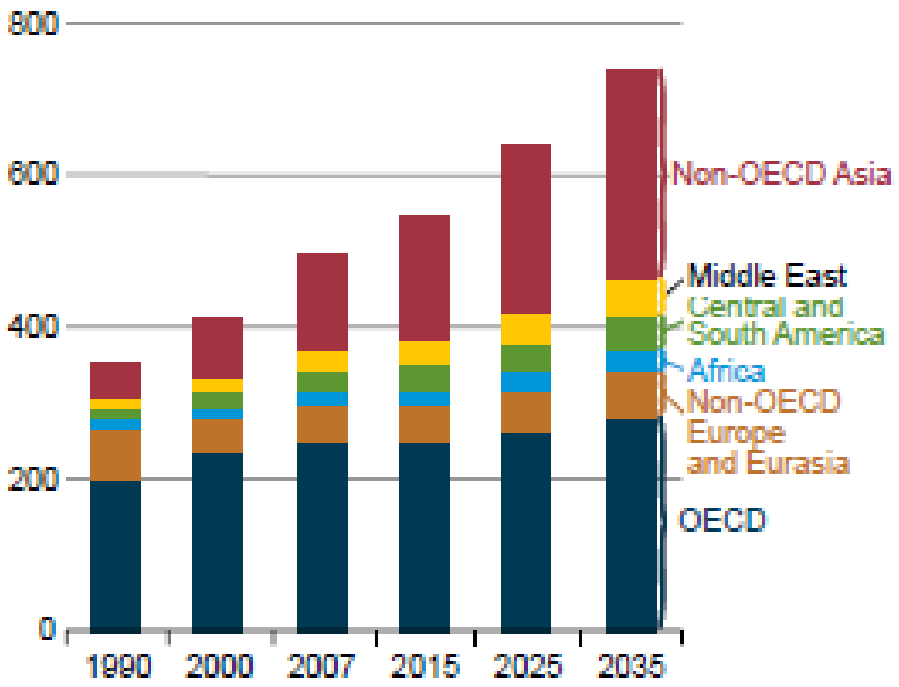

Figure 3: World Energy Consumption 1999-2035 (quadrillion Btu)[3].

1.2 Renewable Energy and Solar:

Finding alternatives to fossil fuels has increased the need for sustainable renewable energy sources. Renewable forms of energy have been around for some time; for instance, hydroelectric power has been in use for decades along with wind and solar. However in 2008, these forms of energy only accounted for approximately 2.9% of the total primary world energy supply[4(p6)]. Here in the United States, the total percentage of energy from these sources has been 3.4%[5(p1)]. As the demand for new energy sources becomes more important, and the threat of global warming becomes a more serious problem, we are seeing a steady increase in the implementation of renewable energy sources. Not all forms of renewable energy are implementable on a large scale. For instance there are increasingly fewer places available to build dams for hydroelectric power, large scale wind farms need to be placed where the effective wind patterns are reliable enough to be cost effective, and solar fields need to be placed in geographical regions that receive ample amounts of sun light per year. Out of these three forms, solar energy has the greatest potential for energy production, as shown in Figure 4[6]. In addition to geological considerations public opinion plays a large part in the implementation of renewable energy, with the most popular form being solar, as shown in Figure 5[7]. We can also see this trend in the increased production of photovoltaic (PV) modules, Figure 6[8], and in the increasing amount of cumulative installed PV capacity worldwide, Figure 7[9]. These trends have moved the department of energy to start a new initiative called the SunShot program. The main objective of this new program is to bring the installed cost of PV solar to $1 per watt[10], nearly a threefold decrease in cost, Figure 8[10].

SOLAR

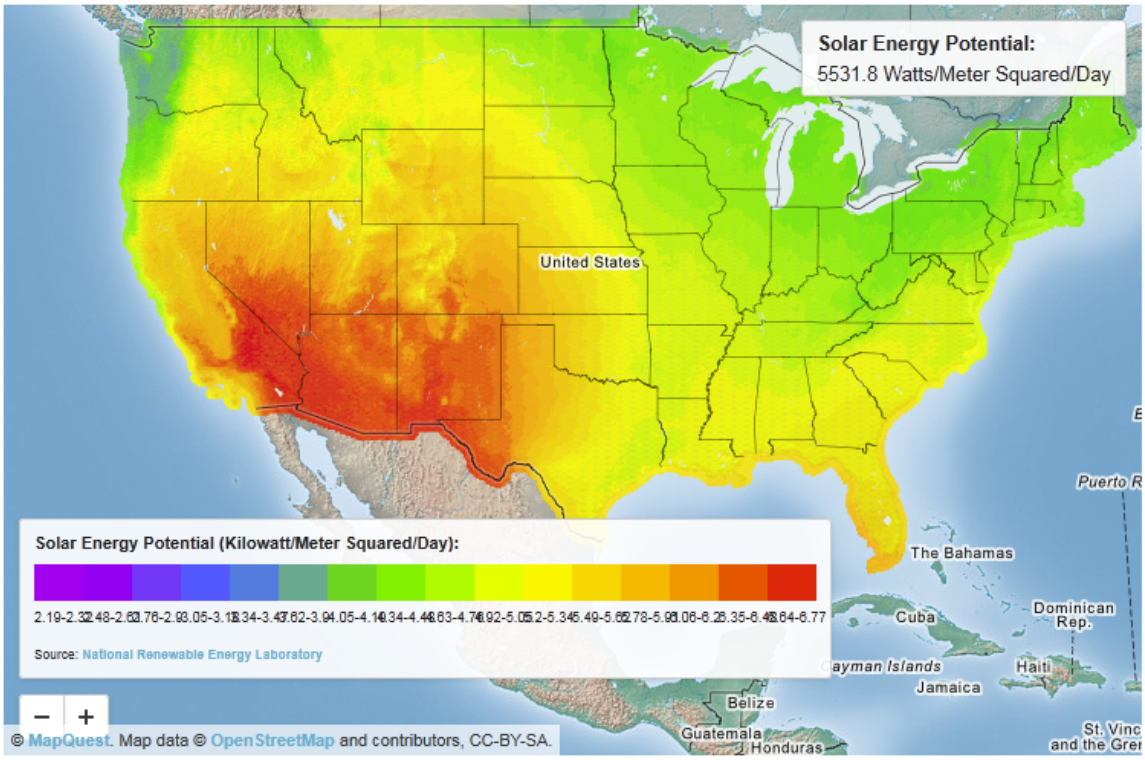

Figure 4: Solar Energy Potential[6].

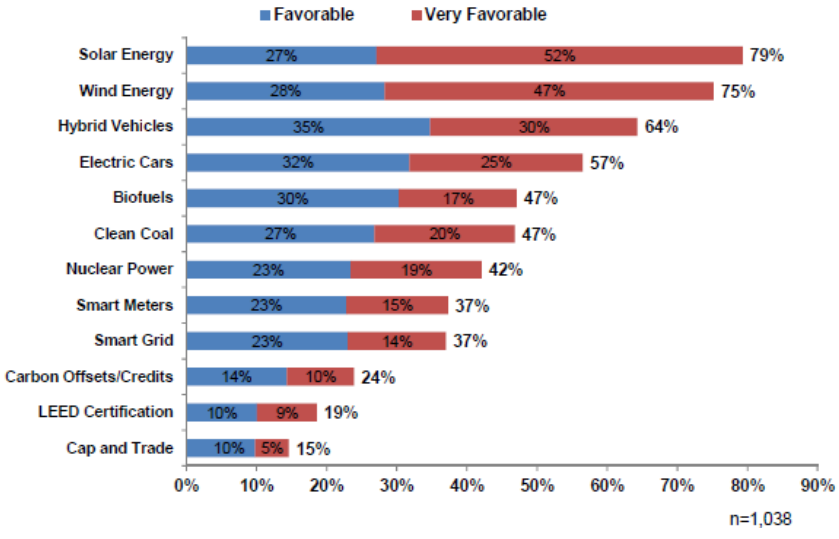

Figure 5: Favorable Impressions of Energy and Environmental Concepts[7].

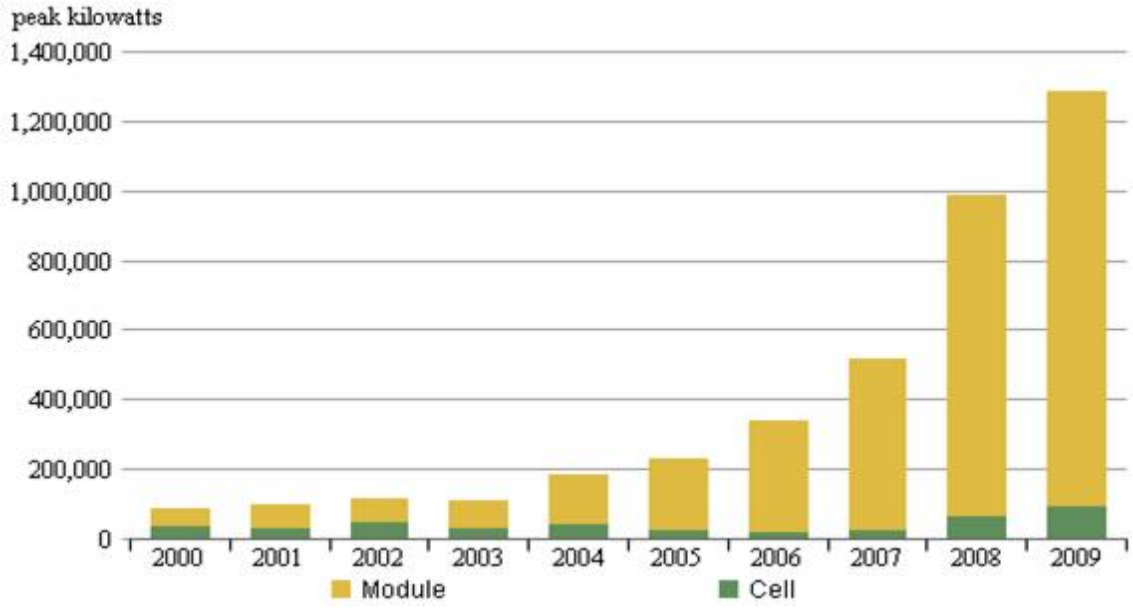

Figure 6: Photovoltaic Cell and Module Shipments 2008-2009[8].

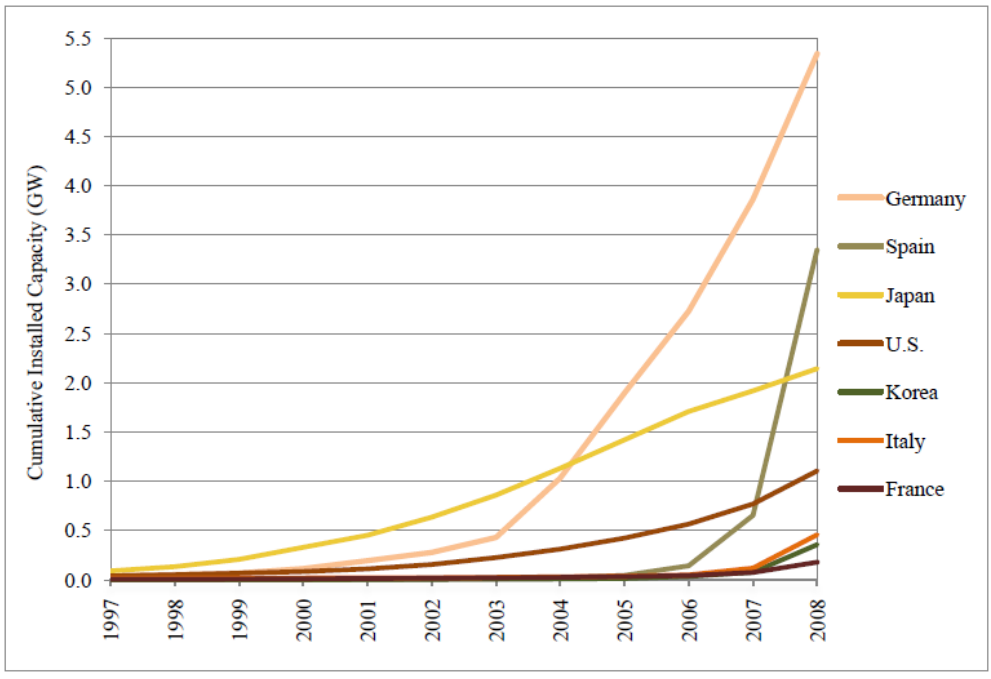

Figure 7: Cumulative Installed PV Capacity in Top Seven Countries[9].

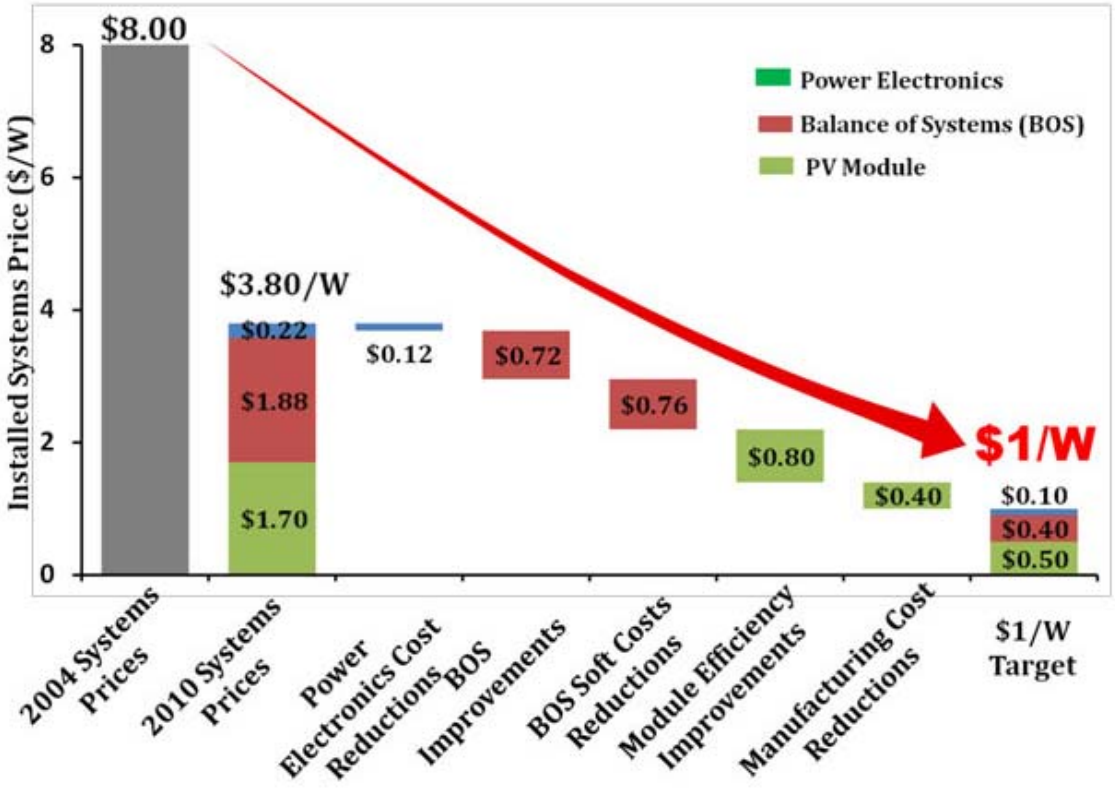

Figure 8: Price Reduction to Achieve SunShot Goal[10].

1.3 PV Solar Cells comparison – Why CdTe.

There are several different types of photovoltaic (PV) solar cells. The most common forms of PV are crystalline silicon (C-Si), Cadmium Telluride (CdTe) thin films and CIGS. C-Si has been the major form of PV technology. However over the last decade CdTe thin film research has improved its efficiency and manufacturability making it a more favorable technology. This can be seen by the 181% per year increase in CdTe production from 2004-2009[11]. CdTe modules also show the lowest cost per watt and are predicted to drop close to $0.50 per watt by 2015, Figure 9[12]. In addition to the lower

manufacturing cost of CdTe modules the greenhouse gas emissions over its life cycle is less than the other major PV solar cell technologies, and it is significantly less than other forms of energy, figure 10[13].

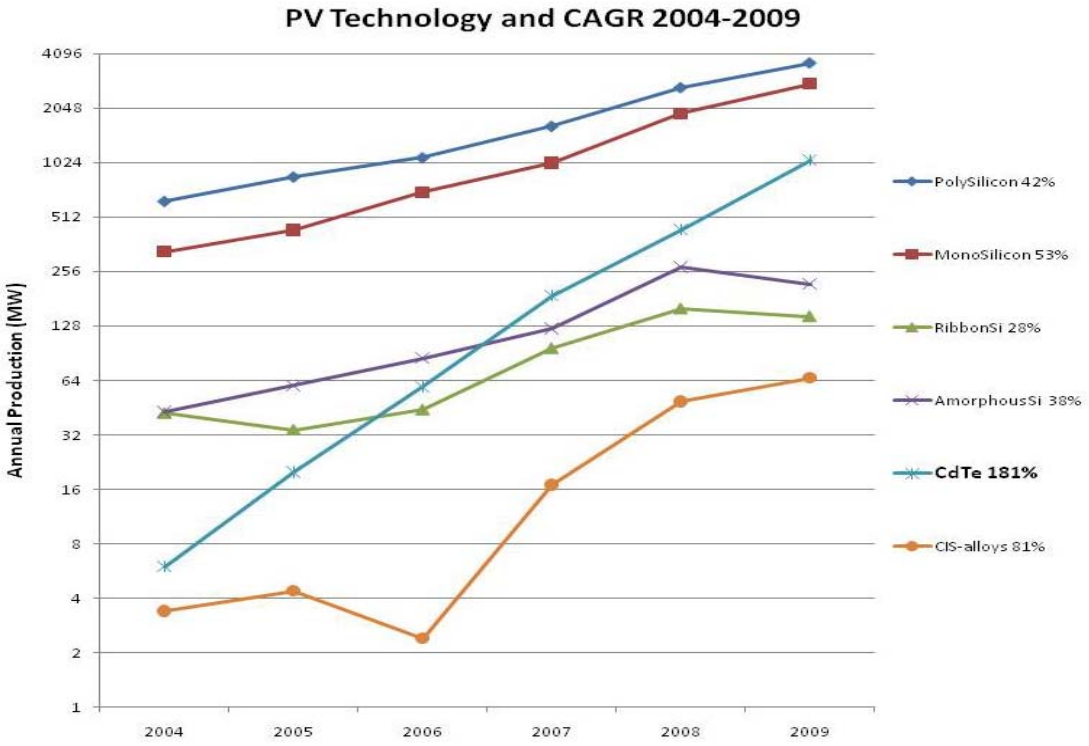

Figure 9: PV Technology and CAGR 2004-2009[11].

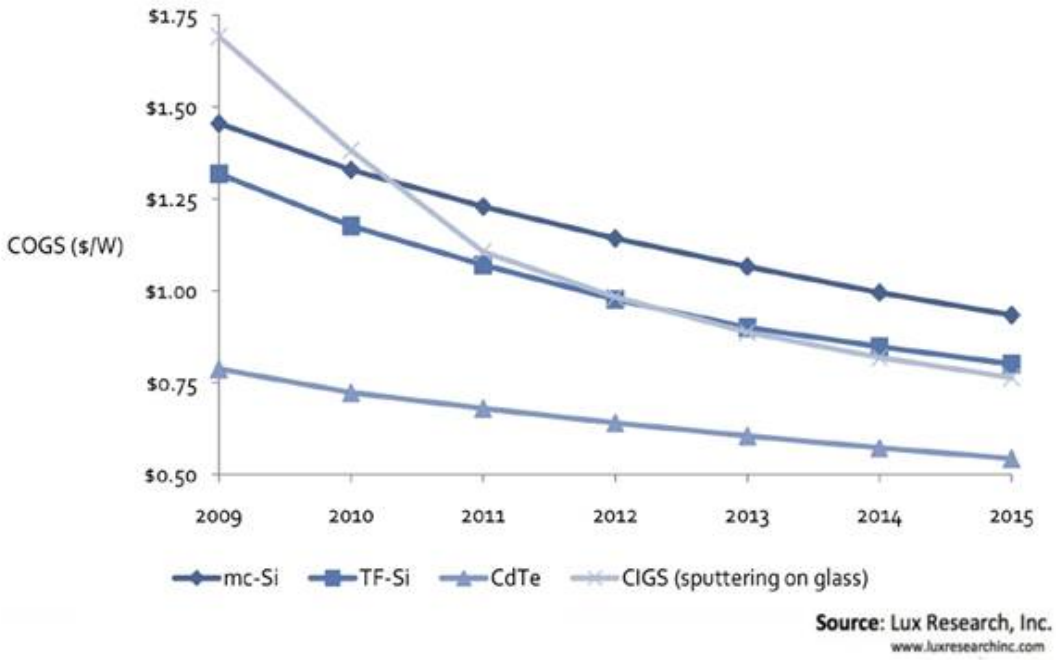

Figure 10: Manufacturing Cost per Watt for Major PV Technology[12].

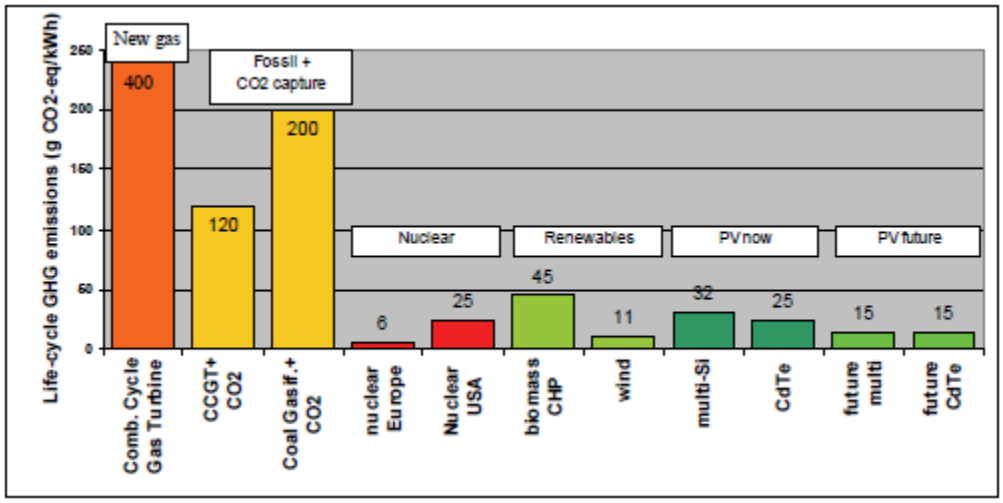

Figure 11: Comparison of Greenhouse Gas Emissions of Different Energy Supplies[13].

1.4 CdTe Thin Film Solar Cells.

Cadmium Telluride (CdTe) photovoltaic solar cells are comprised of four distinctive films deposited on glass. The first layer is a transparent conductive oxide (TCO) used as a front contact for the device. The next two layers comprise the photo diode in which the first layer is Cadmium Sulfide (CdS) and the second layer is Cadmium Telluride (CdTe) the chemical from which the cell structure gets its name. The last layer(s) are used as the back electrode to complete the circuit, Figure 12.

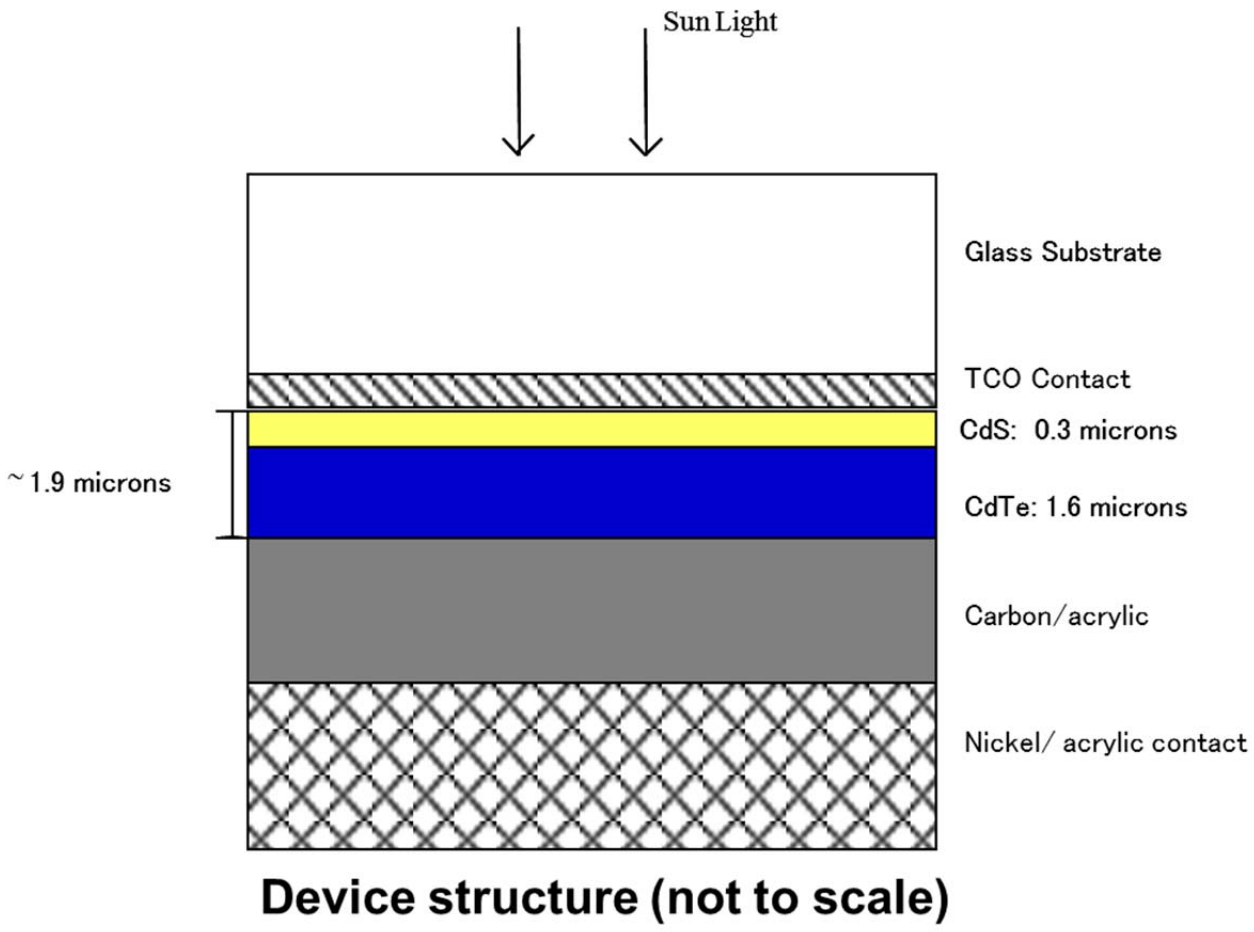

Figure 12: CdTe Device Structure.

1.5 CdTe Device Manufacturing.

There are several ways to manufacture CdTe thin film solar cells. The method of focus for this thesis is the deposition system created by W.S. Sampath, K.L. Barth, and R.A. Enzenroth at Colorado State University. The original system was a continuous inline manufacturing heated pocket deposition chamber that was used to study the manufacturing of CdTe solar cells, as shown in Figure 13[14]. The main features of the system were the air to vacuum to air seals and a continuous substrate transport belt. The main heated pocket deposition source, which is the back bone of the technology, consisted of a graphite deposition crucible and a top substrate heater, with both units were heated by infrared lamps, Figure 14. These key techniques made it possible to produce a CdTe solar cell every 2 minutes and was pivotal in establishing the base technology for mass production of CdTe solar cells which lead to the formation of Abound solar, formerly AVA solar.

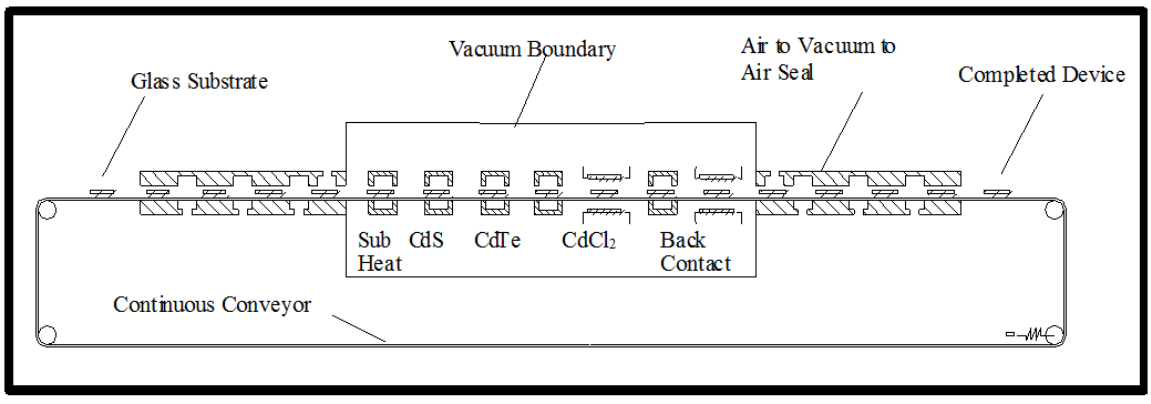

Figure 13: Schematic of Original Pilot System at Colorado State University[14]

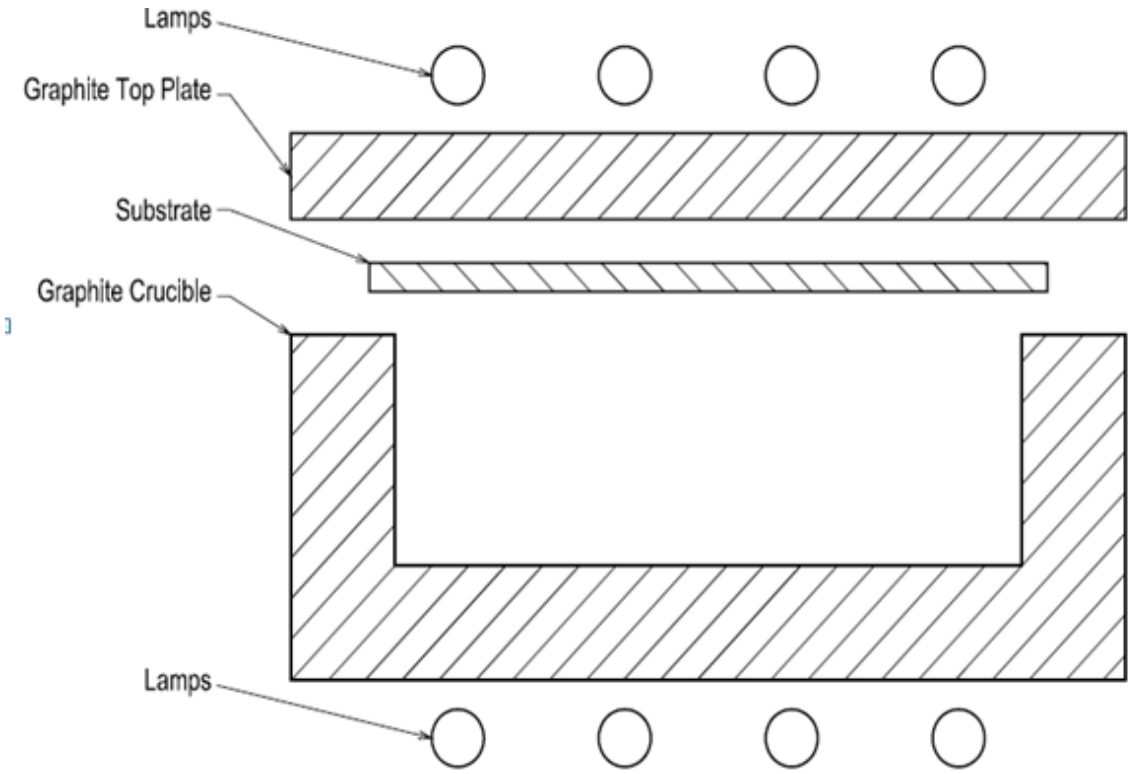

Figure 14: Heated Pocket Deposition Source with IR Heating Lamps

Chapter 2: Motivation behind Modeling.

2.1 Creation of the Advanced Research Deposition System.

The original system had been useful in developing the manufacturing process used to start the PV manufacturing company, Abound solar. However, by 2009 the system had many deficiencies for future research. It was determined that a complete redesign of the system was needed in order to continue research into improving the CdTe solar cell structure. This decision also brought the opportunity to improve the flexibility of the system as a research tool. It was decided to change the system from an inline belt driven system to a single substrate load lock design, as shown in Figure 15. This was a major deviation from the original design and was renamed the Advanced Research Deposition System (ARDS). The load lock design of the new ARDS allows the researchers to change the process time at each station and process sequence itself, opening up the opportunity for future research in the solar cell manufacturing process.

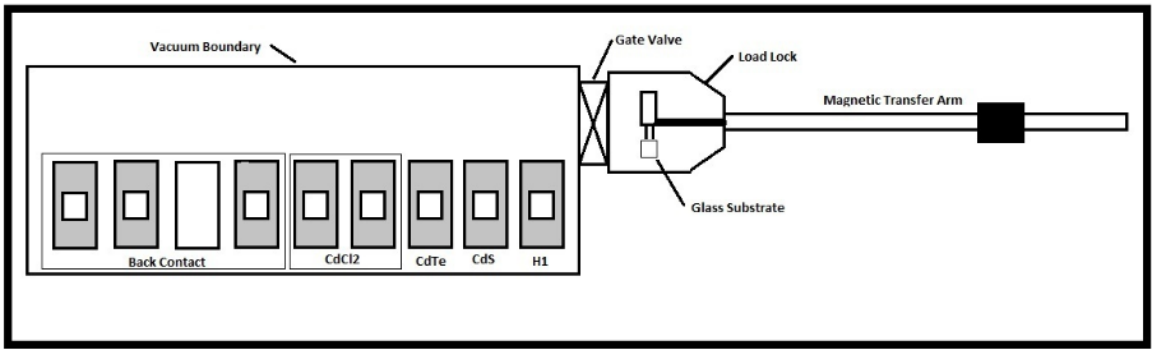

Figure 15: New Advanced Research Deposition System (ARDS).

2.2 Development of the embedded Heating Element Deposition Source.

The re-design of the CdTe deposition system gave the opportunity to change the method of heating used for the deposition system. As stated earlier, the original system used IR heating lamps to heat the substrate heater and the deposition source. The operating range of the system is between 100°C and 620°C. The atmospheric environment of the chamber is 40 millTorr of nitrogen. At these conditions it is typical to use infrared heating to achieve these temperature levels. However, it is difficult to direct all of the radiation to the source. Approximately half of the energy from the IR bulbs is directed at the surface of the graphite source to be heated while the other half is directed at the shielding surrounding the station. This creates excessive heat generation in the shielding, increasing thermal cross talk between adjacent stations. The excessive heat load also damages the shielding and support structure over time creating alignment issues and degrading the efficiency of the shielding. Furthermore, the IR lamps have large power requirements leading to high power consumption and internal chamber arcing resulting in system shut down and additional maintenance. To combat these problems a new form of heating was developed to create the same temperature levels while maintaining thermal uniformity in the source.

The main feature of the design was a NiCr heating element that is potted into the source with a ceramic potting compound, Figure 16. The NiCr heating unit is designed to have a maximum power output of 1.5 kW. This is a significant reduction form the 3kW used by the IR lamp heating method.

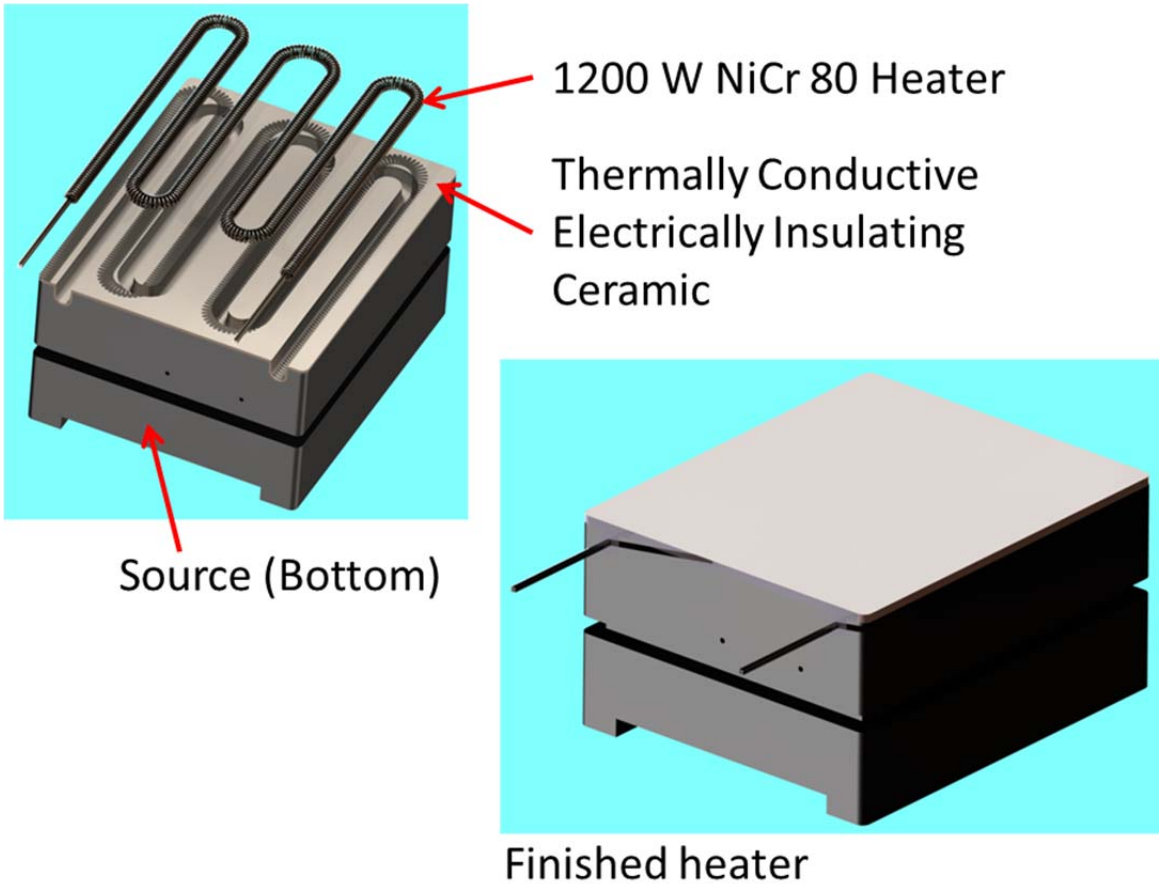

Figure 16: Embedded NiCr Heating for New ARDS Deposition Source.

The new heating method for the ARDS deposition source represented a significant change to original source design. The effectiveness of the new design and the thermal uniformity of the design needed to be evaluated. Traditionally this would involve manufacturing prototypes of the design, outfitting the prototypes with numerous thermocouples, and finally testing the design by evaluating the quality of the film they produced. This process is not only expensive and hard to do on a limited budget, but, in the case of high temperature thin film deposition, where the testing needs to be done in a vacuum chamber, it is difficult to evaluate a new design and requires a well instrumented,

working research tool that has been previously characterized. Due to resource constraints changes to the ARDS had to be fully evaluated without the means of traditional prototyping. It was determined that modern computer modeling would be a pivotal part of the entire redesign of the system in order to achieve the best design quality and performance on a limited budget.

2.3 Modeling philosophy.

The term computer modeling covers a wide array of areas. Its simplest and most wide spread use in computer aided drafting (CAD). Cad drawings allow the engineer to design 3D models of individual parts and then assemble them in the computer to check form and fitment. Mechanical movement can also be implemented in the CAD assembly to check for proper function and clearance with other parts of the assembly. This form of computer modeling has been an integral part of engineering a design for at least the last couple of decades. Other types of computer modeling directly related to the engineering field are; Finite element analysis (FEA) for evaluation of stress, strain, fatigue, created by loading of a part by mechanical of thermal loads, and Computational Fluid Dynamics (CFD) used to determine fluid flow characteristics, combustion patterns, or heat transfer through various media. These modeling techniques are bringing insight into conplex designs. As an example, CFD has been used by companies like Callius Technologies, a Honeywell subsidiary, to model process heater and fired furnaces to improve efficiency and decrease emissions[15]. Various other examples from chemical companies, oil and gas industries, to aviation and transportation industries can be found to support the growing use of computer generated design modeling and evaluation.

Another large motivation for implementing a strong modeling process within the lab was the recommendations given by the National Science foundation. In the report given by the blue ribbon panel on simulation based engineering science (SBES), they state that, “simulation is a key element for achieving progress in engineering and science”, and “SBES has the potential to deliver, within a short design period, designs that are optimized for cost performance and total impact on the environment”[16]. The report goes on to state that it is essential part of predicting design performance and making design decisions without committing resource[16].

Chapter 3: Initial Source Modeling.

3.1 Initial development

The initial concept of imbedding a heating unit was explored by Nicole Luand. Nicole developed the initial track design and showed that it had a potential to create a uniform heat flux across the critical area of the source. From her initial work a method of incorporating a NiCr heating element was developed that would provide 1.2kW of power to the source. Knowing the total available power the concept was then modeled to predict its uniformity and maximum temperature.

3.2 Initial Source Model.

Initial 3D model of the source was created in Fluent. Fluent is a world leading CFD software that is widely used to evaluate fluid flow, combustion and heat transfer.

The initial model was kept simple by only modeling the graphite source itself. Boundary conditions were applied to emulate an unshielded condition where the source is allowed to radiate to a far field at room temperature, Figure 17. The heater was modeled as the ceramic potting compound with the center core remove at the outside diameter of the NiCr coil. The maximum heat flux of the NiCr heating element is applied to the surface of the center core in the ceramic potting compound. This arrangement allowed for the investigation of not only the thermal gradients through the source and the maximum temperature of the un-shielded source, but it also allowed for the evaluation of the

gradients through the ceramic potting compound. This is a critical point due to the lower thermal conductivity of the ceramic.

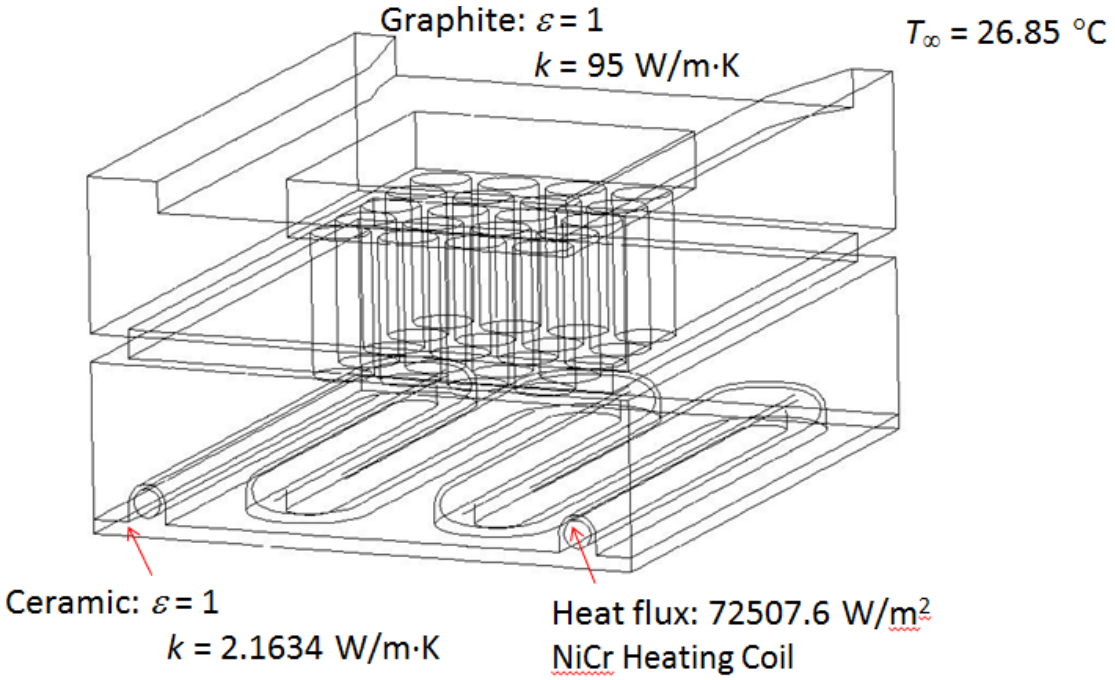

Figure 17: Initial Source Model Layout.

3.3 Results from Initial Model.

Three major finding came from the results of the initial model, Figure 18. First, it was determined that the gradient across the ceramic did not cause the temperature of the NiCr wire to raise above its operating threshold of 1200°C. In addition, the ceramic caused no effect on thermal uniformity. Next, the model predicted a very uniform temperature across the pocket with no noticeable gradient. This is a critical finding that suggests that the temperature of the chemical sublimation will be even across the source. Finally, the initial model suggests that the source will come to a maximum temperature of approximately 505°C at the location of measurement within the source used for thermal control. This is lower than the target minimum of 620°C that is required to sublime CdS.

It was determined that the model should predict a lower steady state temperature when modeled without shielding. This model gave the confidence to proceed with the initial prototype to test the manufacturability of the embedded NiCr element and operation.

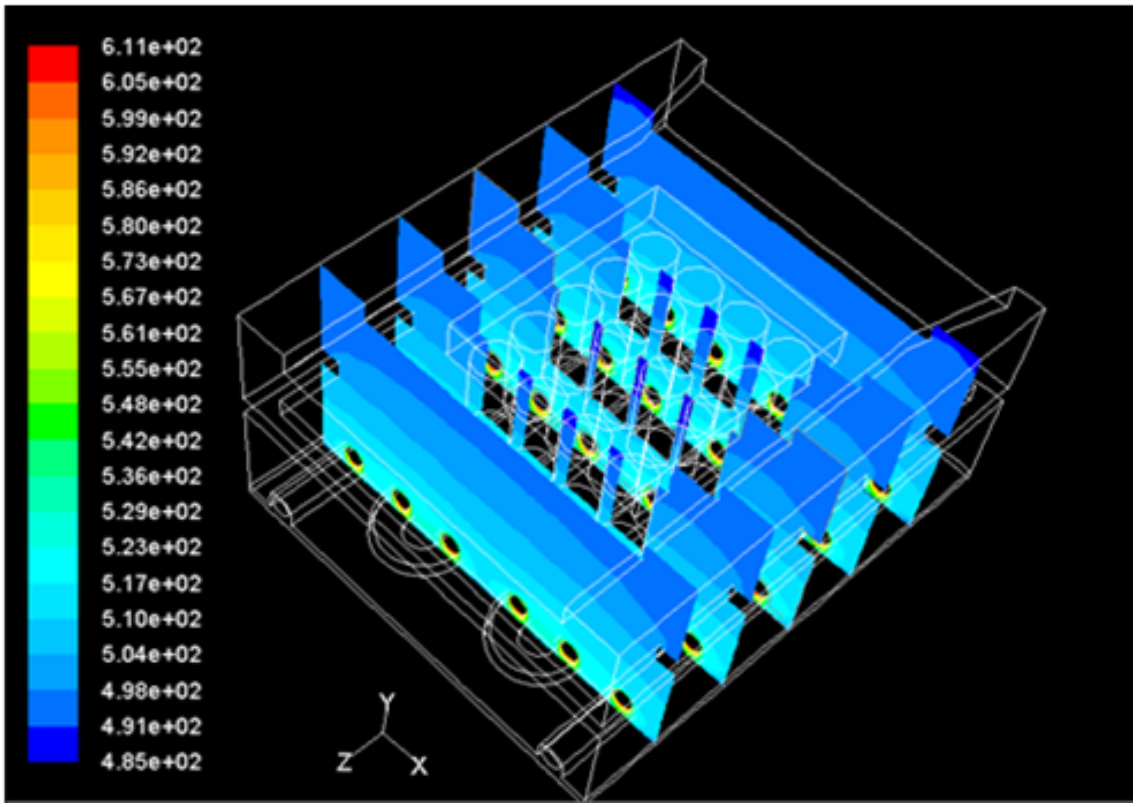

Figure 18: Results of Initial Model. Temperature in °C shown on left.

3.4 Initial Prototype.

The initial prototype did not contain the complex geometry of the sublimation wells and pocket of a full source. The main focus of the prototype was to test the viability of the embedded NiCr heater design, Figure 19.

Figure 19: Prototype of the Embedded NiCr Heater

Two tests were performed using the NiCr heating unit prototype. All tests were done under vacuum in a non-cooled test chamber. The first test was done without shielding, Figure 20. This test proved that the concept would work. The heating unit stayed intact and did not dislodge from the graphite source. In the initial test, the prototype was driven to 525°C until the chamber began to overheat. At this point the rate of temperature increase had dropped to an almost steady state condition. It was noticed that when looking at the same location in the model as the control point in the prototype, the unshielded model and the prototype are within 10°C.

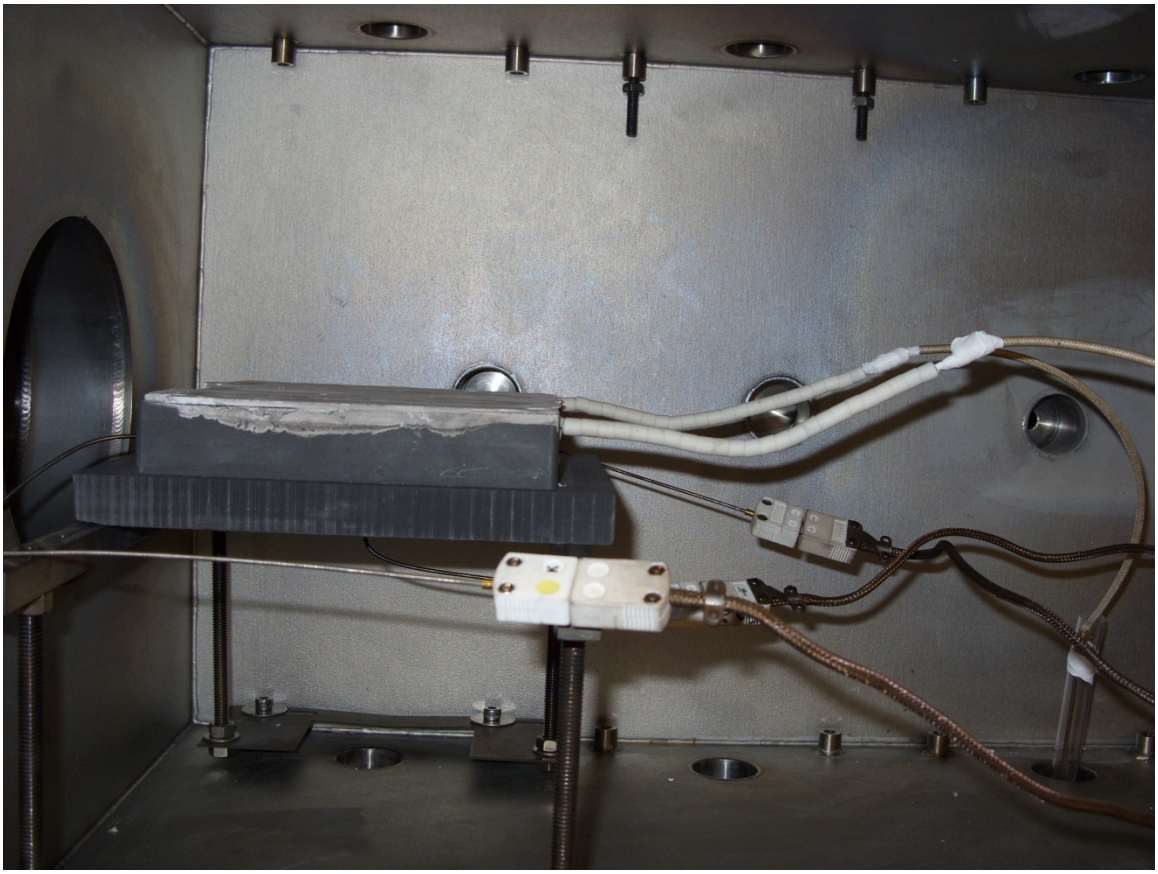

Figure 20: First Prototype Test without Shielding.

The second test involved adding shielding to the prototype, Figure 21. The shielding allowed the prototype to reach a temperature of 640°C before the chamber began to overheat. This suggested that the design would work for the entire range of process temperatures. From this testing the designs were finalized and the order placed for a full set of chamber sources.

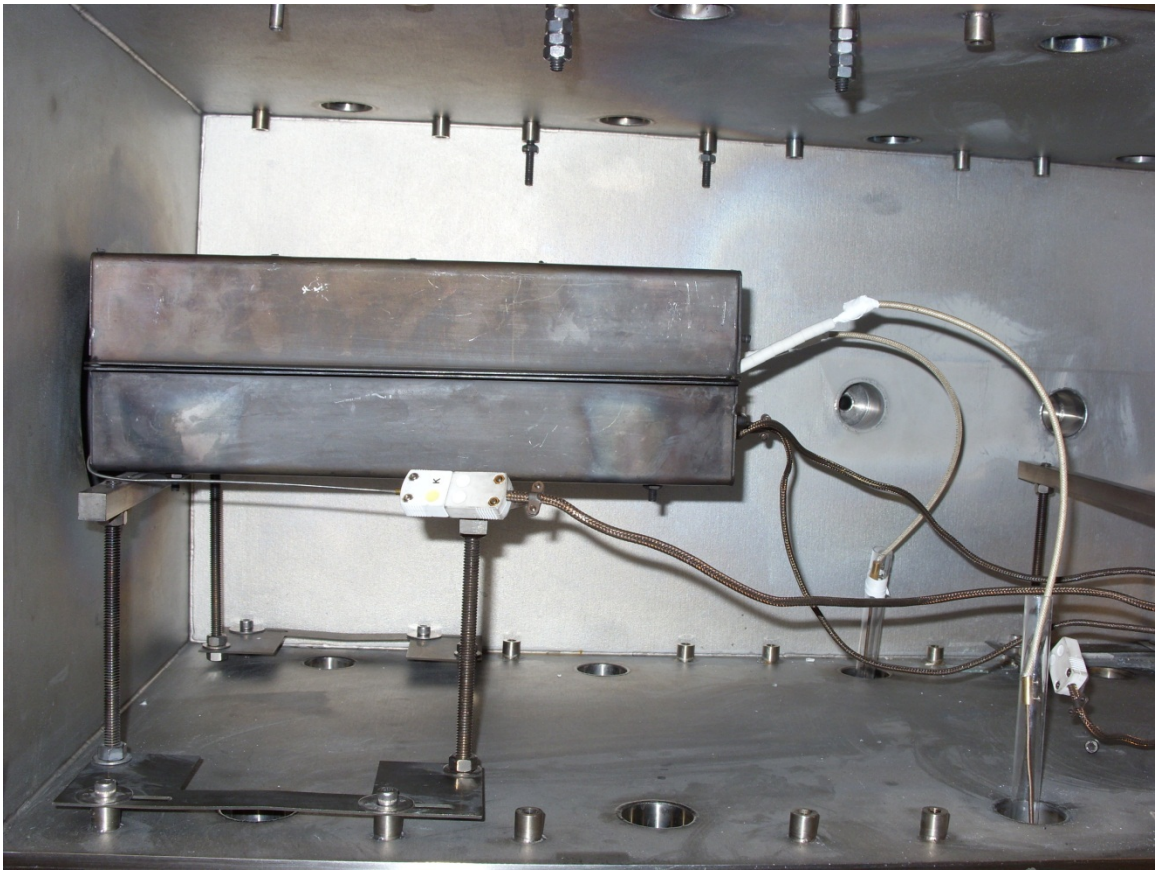

Figure 21: Prototype with Shielding.

3.4 2D Model.

A 2D model of the cross section of the source including the mounting box, enclosure, and shielding was attempted. This form of model allowed the use of symmetry and modeled radiation to the enclosure. The radiation model used in Fluent was the Discrete Transfer Radiation Model (DTRM) where radiation leaving the surface is approximated by a given number of rays within a range of solid angels[17]. The number of rays is defined by the number of divisions θ and ϕ, Figure 22.

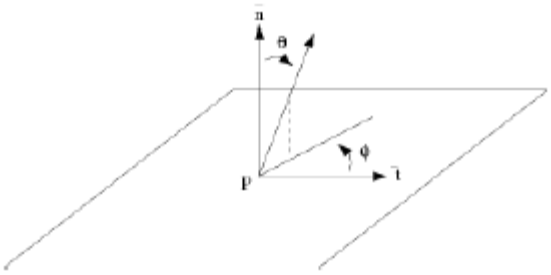

Figure 22 : Angels θ and ϕ Defining the Hemispherical Solid Angle About a Point P.

3.5 2D Model Results.

The results from the 2D models still suggested uniform temperature through the critical zones of the source. The overall temperature predicted by the 2D models was well over the temperature of the initial 3D model and the initial test done on the prototype, Figure 23.

In a 2D model, the depth of the model is not meshed. The theoretical faces in the depth of the model are essentially treated as adiabatic surfaces where there is no loss or addition of energy. In the case of a small source, the loss of energy by the faces not accounted for in the 2D model causing the model to predict a high than normal steady state temperature. It is therefore concluded that 2D models cannot be used for small sources where the depth is close to the same dimension as the cross sectional width.

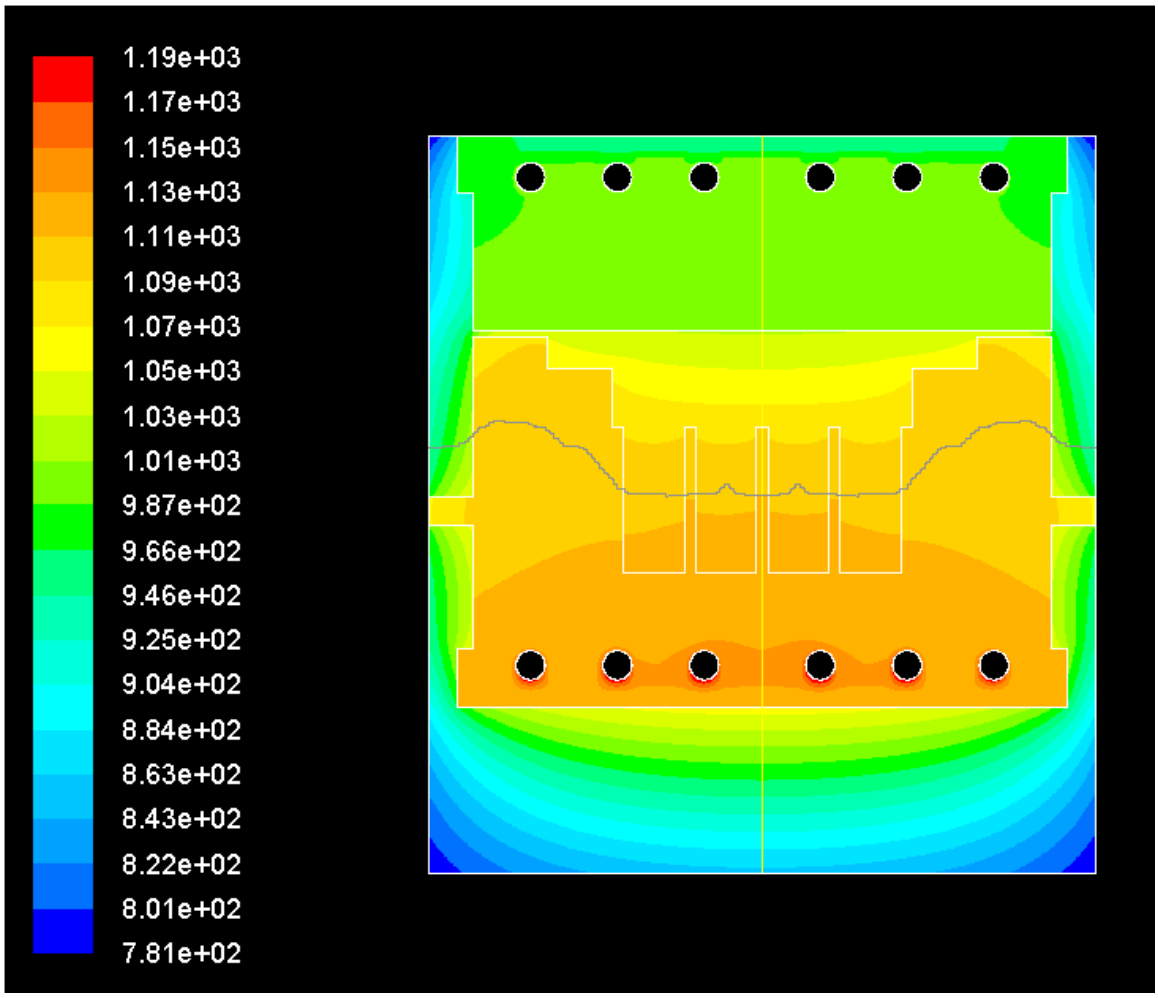

Figure 23: Results from 2D Model. Temperature in °C shown on left.

Chapter 4: Basic 3D Model of Source with Enclosure.

4.1 Main Configuration of the 3D Source Model.

The next step was to model the source in greater detail. This involved modeling both the top heating source and the bottom deposition source along with the supporting structure, Figure 24.

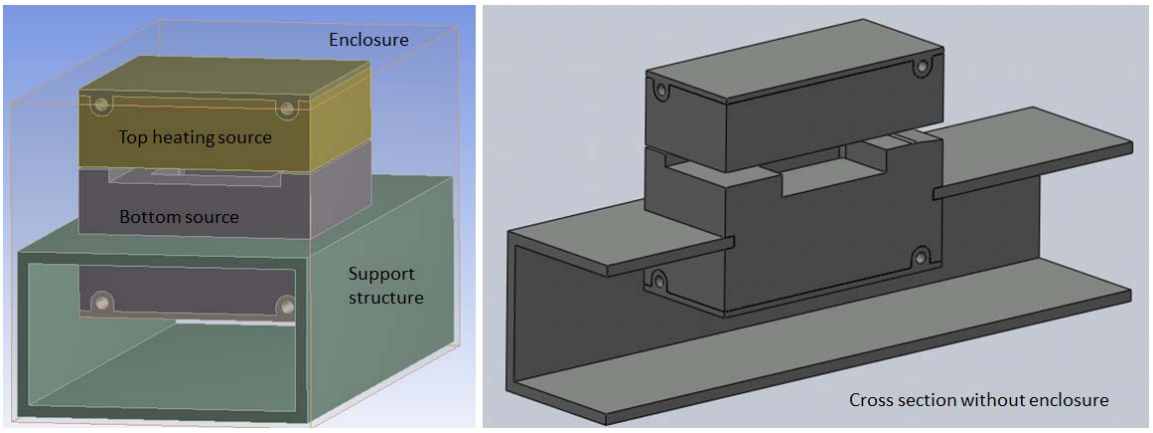

Figure 24: 3D Source Model.

This model also represents the source configuration used for the initial heating station. For the heating station a source is made without the chemical wells. This was also the first source completed, and as such the first source to be tested in the test chamber. The heating station does not contain a shutter or any additional shielding making it the simplest source in the system. The main exterior shielding was also not installed during testing and thus it was left out of the model.

4.2 Basic 3D model details.

The heater contains the same core at the diameter of the NiCr heating coil, in which either a constant temperature or constant heat flux is applied.

The material properties for all materials are determined from the specifications of the manufactures. The outer wall of the enclosure is set to radiate to an external far field temperature of 26°C and emissivity of 1.0. The atmospheric environment is set to the typical system operating pressure 5.33Pa nitrogen.

It was determined that the settings for the deposition station of CdS should be used for testing because they represent the highest temperature in system. These settings also have the largest gradient between the top heating source and the bottom deposition source, which are 400°C and 620°C respectfully. It was understood from the previous 3D models that an unshielded source would be able to reach the 400°C setting for the top; therefore, the heater surface for the top heating source was set at a constant temperature of 400°C. The bottom source was given the maximum heat flux of the NiCr heating element which is 72.5kW/m^2, Figure 25.

4.3 Basic 3D Model Results.

The basic model was run with a steady state solver to determine the maximum steady state temperature achievable by the bottom deposition source, and in transient mode to determine the time necessary to come to the desired operating temperature. These first runs were done in a unshielded form to match the test conditions of the first full source tested.

The results from the model show that the bottom source came to a steady state temperature of 555°C while the upper heating source came to a steady state temperature of 415°C. The experimental testing was done with the following set points; top heating source set point – 400°C, bottom deposition source set point – 620°C.

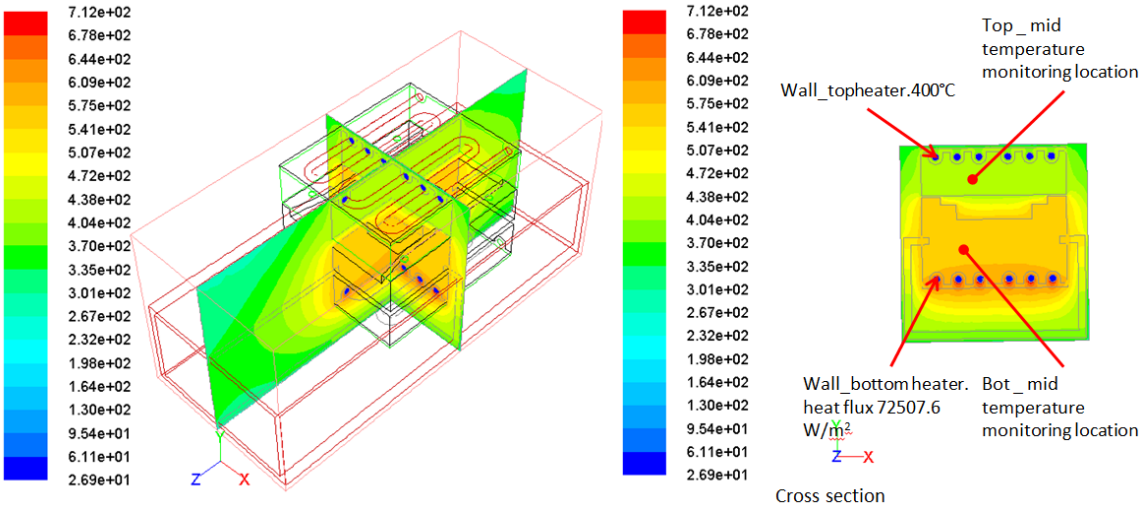

Figure 25: Result Images and Layout of the Basic 3D Model. Temperature in °C shown on left.

The testing was done in the same non-cooled test chamber used for the prototype testing. Because the test chamber did not have any means of cooling, the test could only be run for approximately 75 minutes before the outer skin of the chamber overheated. The results of the test indicate that the temperature rise in the top heating source had reached the set point and that the controller was able to keep the temperature within ±10°C, as shown in Figure 26. The temperature in the bottom deposition source had not completely come to steady state, but the rate at which the bottom source temperature was increasing had significantly decreased.

From the graph of the experimental data it can be seen that the racking holding the source and both the bottom and top of the test chamber are still increasing in temperature at a much greater rate than the bottom source. Heating of the chamber is not accounted for in the model. The far field of the model is held at a constant temperature of 26°C, whereas the test chamber wall cannot be held at a constant temperature. This condition would allow the bottom source to show higher temperatures than the model predicted. The predicted steady state temperature should be approximately 558°C, 8°C higher than the measure temperature. Considering that the data shows the temperature of the source is still increasing, it is reasonable to conclude that the model and experimental data are within reasonable agreement.

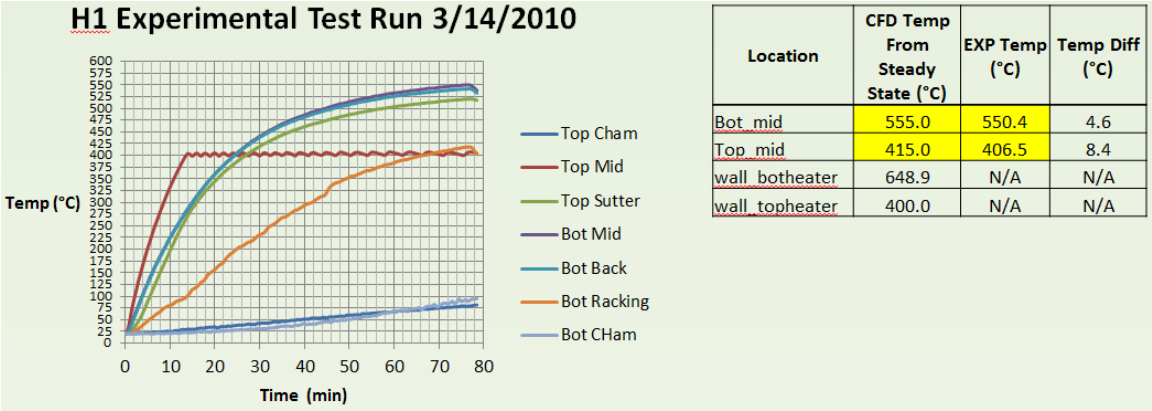

Location	CFD Temp From Steady State (°C)	EXP Temp (°C)	Temp Diff (°C)
Bot_mid	555.0	550.4	4.6
Top_mid	415.0	406.5	8.4
wall_botheater	648.9	N/A	N/A
wall_topheater	400.0	N/A	N/A

Figure 26: Experimental Test Run vs. Model Temperature

The transient run results shows the model predicted that the both the top and bottom sources would reach a steady state condition 10-20 minutes quicker than the actual measured temperature suggests, Figure 27. This difference is due to the fact that the material properties used in the model do not account for the dynamic increase in the specific heat of the graphite and other materials.

Dynamic material properties can be used in the Fluent CFD solver and improve the accuracy of the transient calculation. However, it was determined that the transient calculation did not have any beneficial use to the design process at this time and further evaluation of the transient model was not needed.

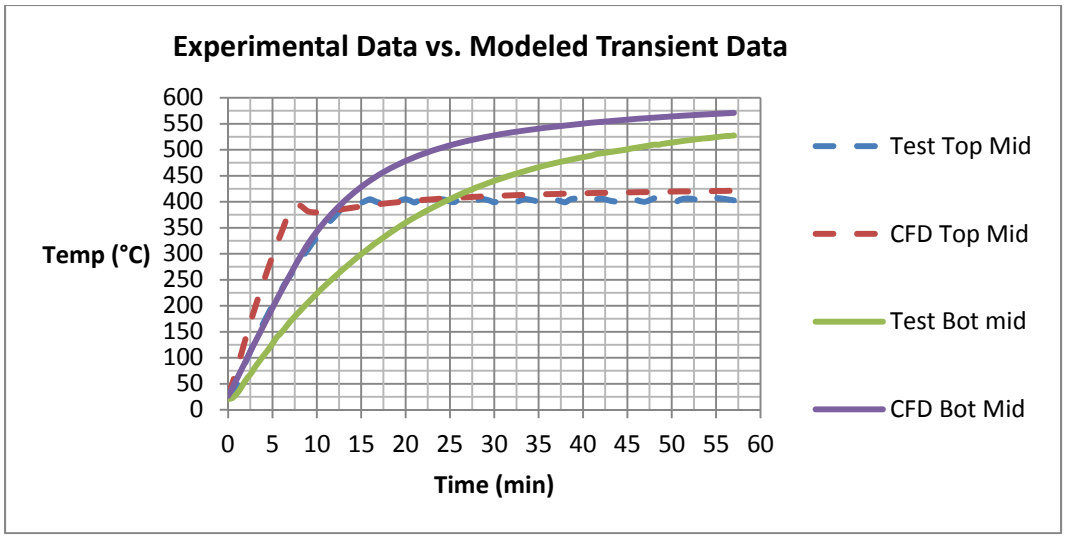

Figure 27: Experimental Data vs. Modeled Transient Data.

4.4 Basic 3D Model Used to Evaluate a Shield Approximation Technique.

Once the assembly of the ARDS had been completed, characterization of the system through film quality had begun. During this process it was determined that the top heater for the CdS station was being thermal driven to a higher temperature than needed by the bottom deposition source. Measurements of the driven source indicated a driven temperature of approximately 494°C. The boundary conditions for the surfaces of the top heater and bottom deposition source were modified in the model to approximate the effects of shield. This was done by dropping the emissivity of the surface from the typical emissivity of graphite, 0.8, to that of the stainless steel shielding, 0.4. The model was then run with the bottom deposition source heater set at a constant temperature that will produce the same set point temperature for the CdS station, Figure 28. The driven top temperature in the model was within 10°C of the measured temperature. This shows that shielding can be approximated by modifying the emissivity of the surface of a part.

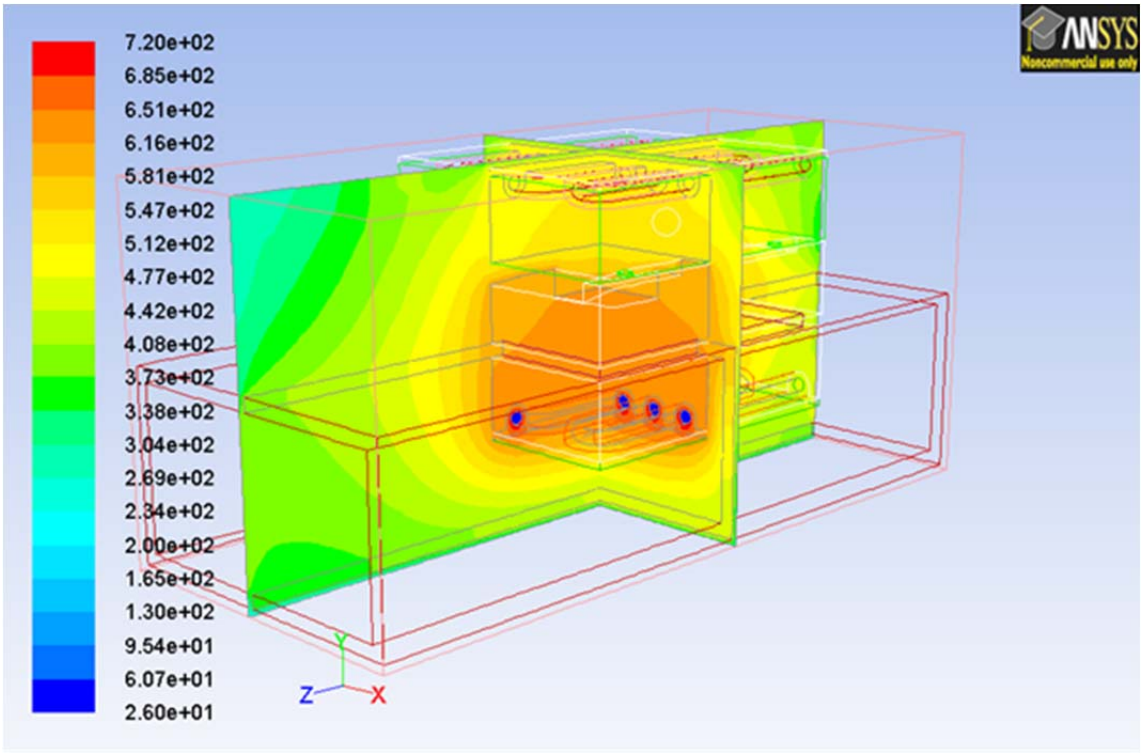

Figure 28: Model of the CdS Station Parameters Showing Driven Top Temperature Effect. Temperature in °C shown on left

Chapter 5: Next Generation Top Source Modeling.

5.1 The development of the Next Generation Top Source Design.

As stated in the previous chapter, the temperature of the top source for the CdS station was being driven above the desired set point by the bottom deposition source. The desired temperature was 350°C or less. The driven temperature was 494°C. Several design changes were implemented to try to drop the driven temperature. These changes included the addition of shielding between the top and bottom source along with removing the shielding from around the top source. The changes decreased the driven temperature to approximately 423°C. It was determined that the top temperature could be further decrease by increasing the surface area of the top source that views the colder chamber walls allowing for increased heat loss through radiation. The effectiveness of the concept and to determine the amount of area increase needed was modeled to decrease the amount or eliminate the need for prototype testing.

5.2 The Next Generation Top Source Model.

The model consists of the source itself without an enclosure. The heat flux into the surface that faces the bottom deposition source was calculated from the measure data and applied as a constant heat flux into the part. All other surfaces were set to radiate to an appropriate far field condition with the standard emissivity of graphite, 0.8. The heat spreader part of the new top consists of a flat plate added to the top of the heating source, Figure 29. The thickness of the additional heat spreader as well as the front, back, and

side overhangs were parameters that could be modified for evaluation. Repeated running of the model was done until the best combination of parameters was found. It should be noted that interference with other internal parts was also under consideration when determining the size of the additional heat spreader plate.

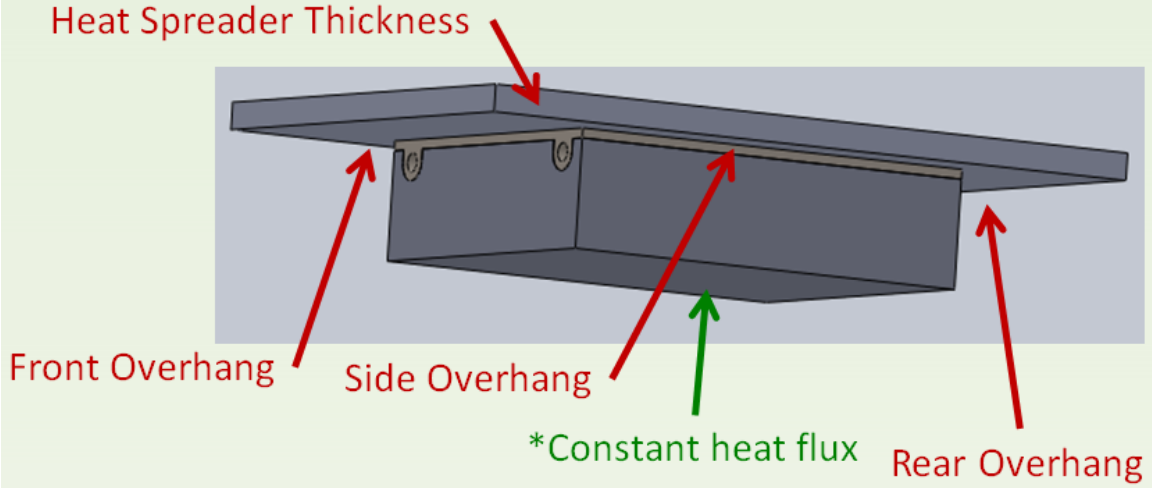

Figure 29: Next Generation Top Design.

5.3 Concept evaluation results.

First the model was run without the additional heat spreader plate as a benchmark for evaluation, Figure 30. The bench mark run indicated a temperature of 440°C at the bottom surface of the part and an approximate temperature of 424°C at the control thermocouple location within the part, which is 0.5” from the bottom surface. This sets the model to match the measured conditions of the system. The model was then run with different parameters until a final parameter set was finalized, Figure 31. The final design indicated that the bottom surface could be held at an approximate temperature of 354°C, with an approximate control point temperature of 345°C.

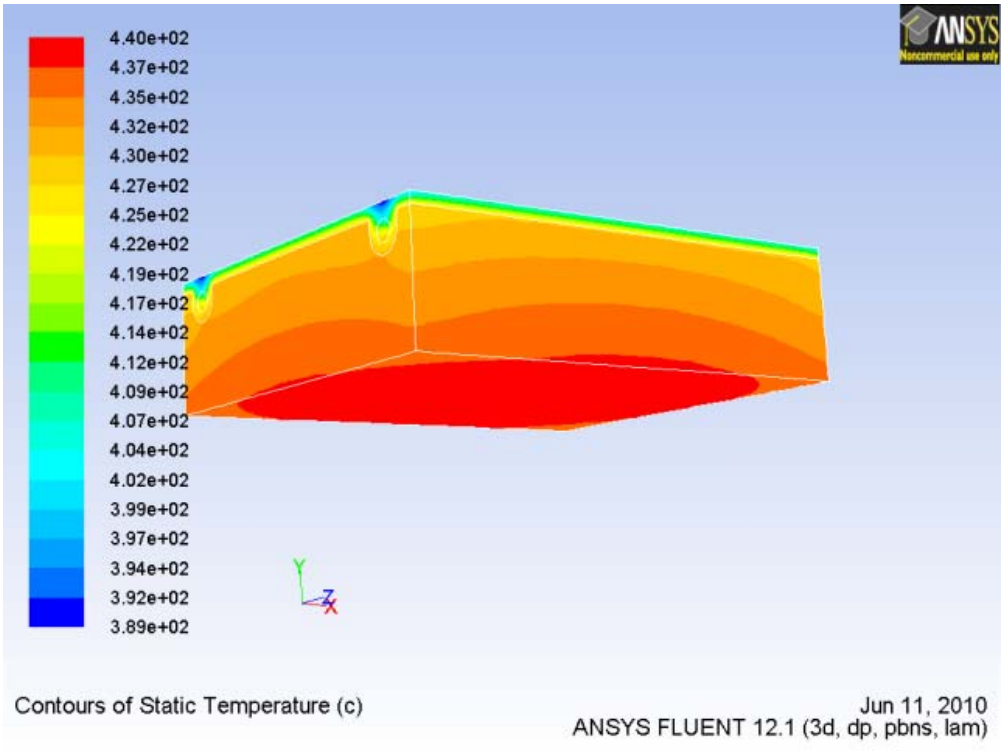

Figure 30: Benchmark of the Top Heating Source for Comparison. Temperature in °C shown on left

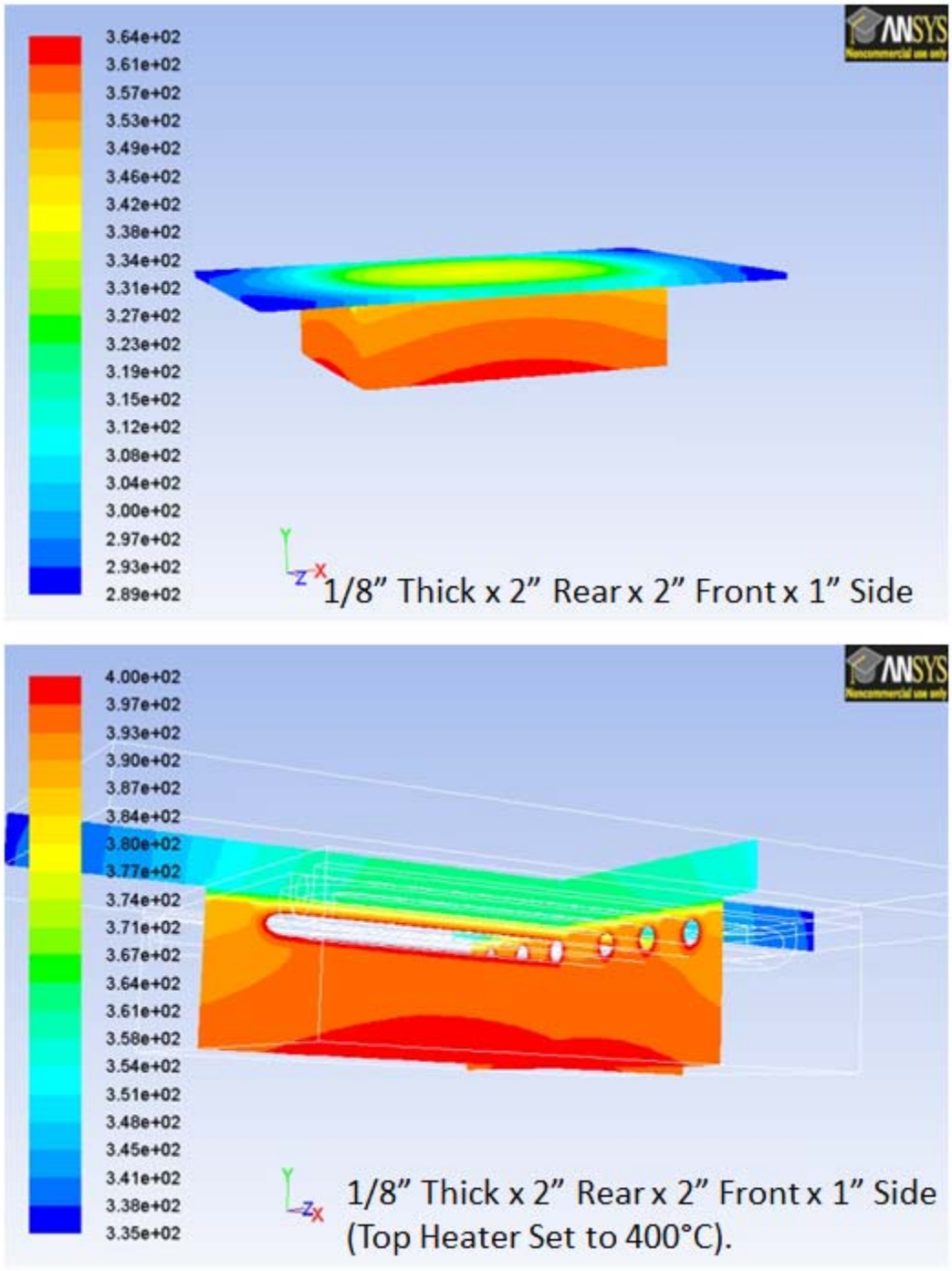

Figure 31: Next Generation Top Source Evaluation. Left: One Design Parameter Set. Right: Final Design Parameter Set. Temperature in °C shown on left

5.4 Final design of the Next Generation Top Source.

During the fabrication of the top heater, adding an additional heat spreader plate to the top of the existing sources was determined to be impractical. A completely new top heating source was designed from the parameters set from the concept modeling. The new source deviated from the original design by completely integrating the heat spreader plate with the source and changing the design of the embedded heating unit. The new design of the embedded heater proved more robust and easier to manufacture than the original design, Figure 32. The final design was modeled to determine that effects of the changes, Figure 33. The model predicted a driven temperature, at the control thermal couple location temperature, of 348°C. The actual driven temperature during testing was measured to be 330°C, 18°C less than the modeled temperature.

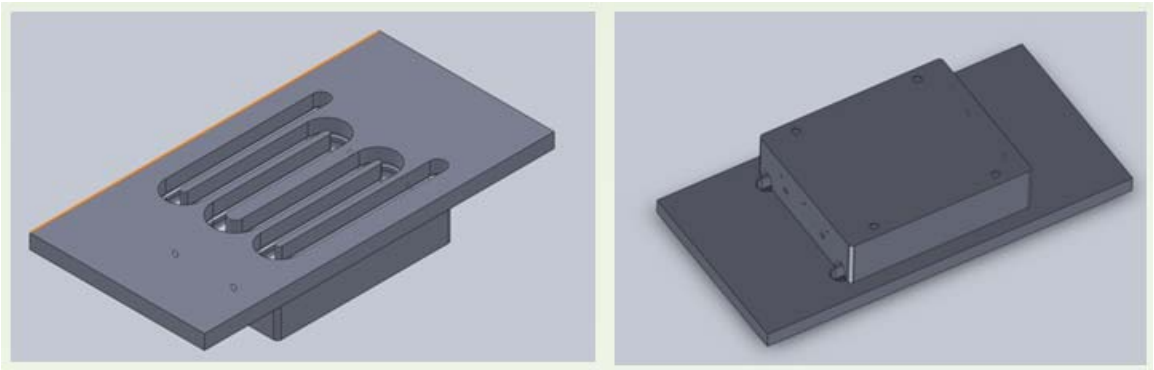

Figure 32: Final Design of the Next Generation Top Source.

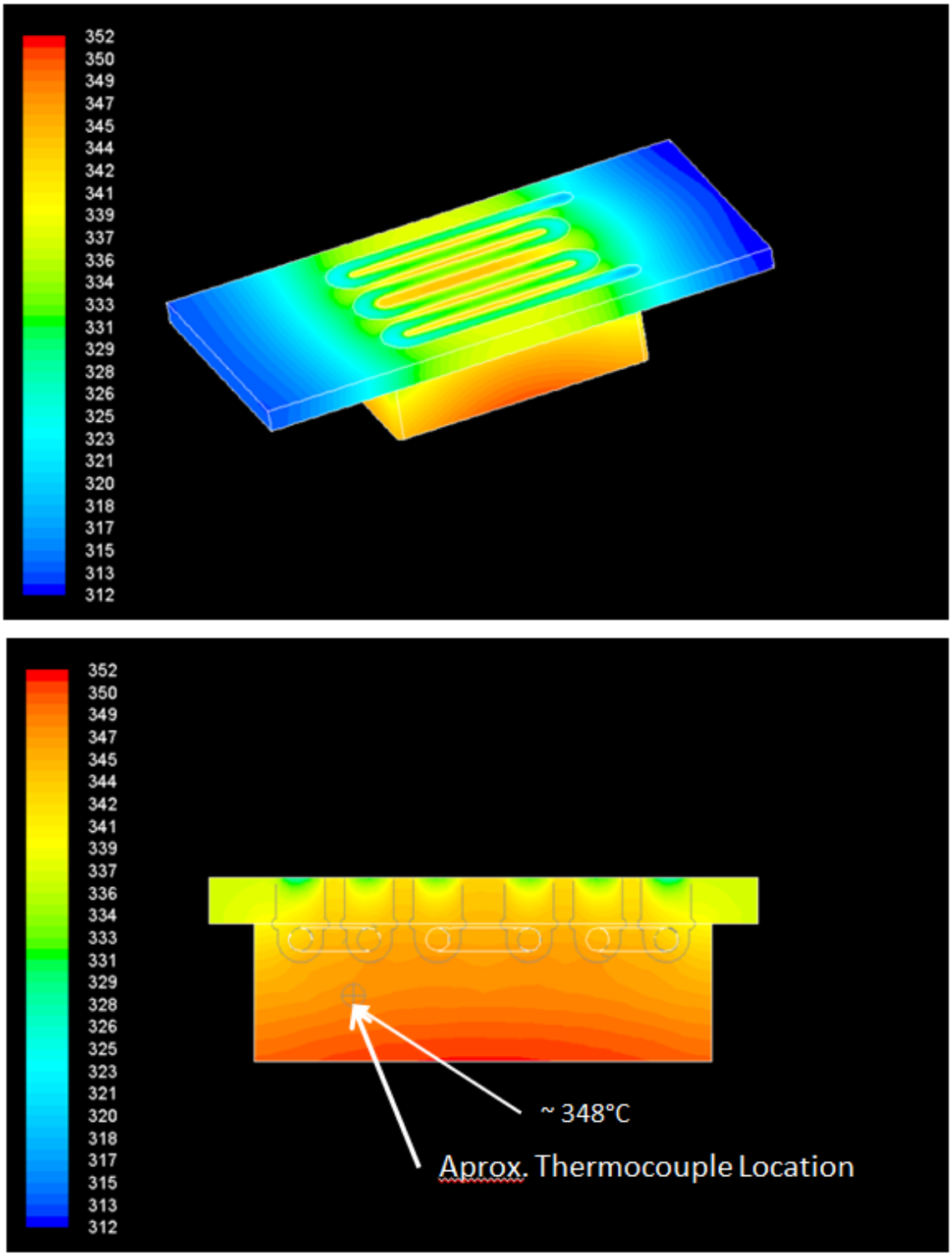

Figure 33: Results of the Next Generation Top Source the Final Design Model. Temperature in °C shown on left

Chapter 6: Detailed 3D Model of the Deposition Station.

6.1 Motivation for Detailed Model.

There are two main reasons for the creation of a more detailed model of a deposition station. In the chemical stations, a shutter is used to block the release of chemical from the deposition source when not in use. The main point of interest is to evaluate the shutter temperature in a deposition source. The other motivation driving the creation of the model is to further evaluate the shielding approximations used in previous models and to get a better approximation of the thermal uniformity through the station under more complete and detailed conditions, Figure 34.

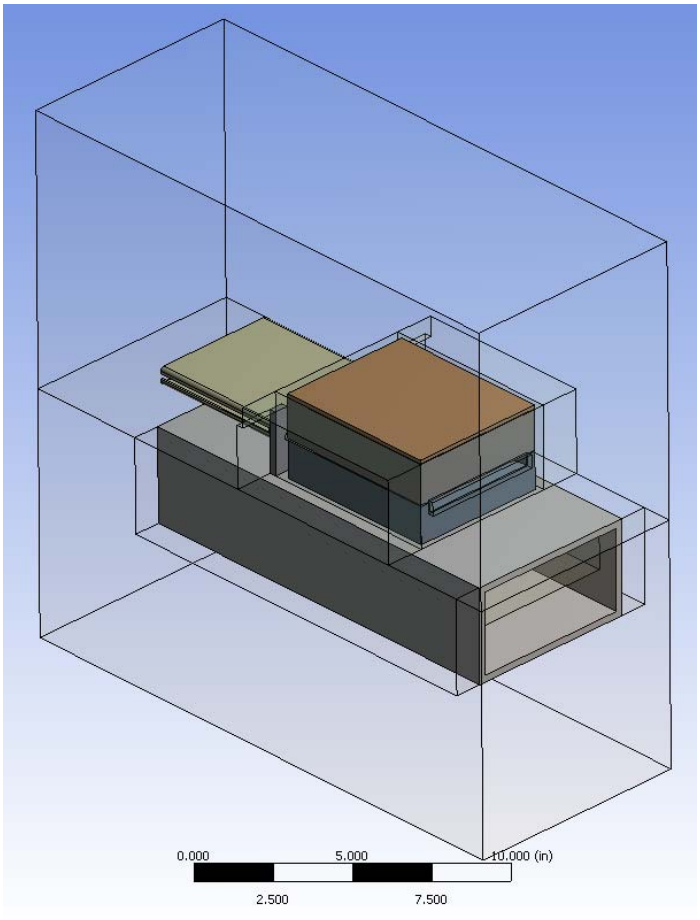

Figure 34: Detailed 3D Deposition Source Model.

Also notice in Figure 34 that the outer surfaces of the enclosure has been segregated so that different boundary conditions can be applied to approximate the temperature of adjacent stations and racking components.

Each deposition source contains a shutter that closes off the pocket to keep the chemical from diffusing out of the station contaminating other stations and the system. In the original belt system, there was always a substrate positioned over the deposition source keeping the chemical within the source except during motion. In the new system, where the substrates are moved through the system one at a time, a method of closing off the deposition source when not in use was needed. The shutter design uses a simple

counter weight device that keeps the shutter over the pocket. When the source is to be used, the incoming substrate pushes the shutter out of the way. When the substrate is withdrawn, the counter weights pull the shutter back into place.

The shutter itself rests on the top of the bottom deposition source and is thermally coupled to it through radiation heat transfer. It was known in the original design concept that the shutter may not come to a high enough temperature to inhibit the condensation of chemical on to it. Subsequently the shutter was designed with a shallow pocket on the underside to collect the chemical and avoid interference due to build-up. This method work well in the CdTe and CdS stations, but in the $CdCl_2$ Passivation station, the buildup limits operation of the system to 6 total substrates.

The detailed model will allow for the evaluation of the shutter temperature and will be used to evaluate design changes to mitigate or eliminate the buildup of chemical onto the shutter.

The shield approximation used in previous models was done by dropping the emissivity of the outer surface of the part that is shielded. This method has proven itself as an easy and quick method of approximating the effects of shielding; however, its overall accuracy had not been evaluated. The detailed model contains provisions to more accurately approximate the shielding using the thin wall conduction approximation in Fluent. The method is done by creating an inner surface in the nitrogen fluid zone at the correct location and in the shape of the shield. This inner surface can then be given a designated material and thickness that the numerical solver will use to solve the temperatures.

6.2 Result from the Detailed 3D Model Centered On the Shutter.

The model was run with the set point parameters for the $CdCl_2$ station to evaluate the temperature of the shutter and its guide. The results can be seen in Figure 35. The model shows that the steady state temperature of the shutter comes to a temperature of 370-380°C. In order to avoid condensation of $CdCl_2$ onto the shutter, it would need to reach a temperature of approximately 425°C. This clearly shows that there is chemical deposition onto the shutter throughout while the station is at operating conditions. It can also be seen from the model that the shutter guide is acting as a heat sink conducting heat out of the shutter.

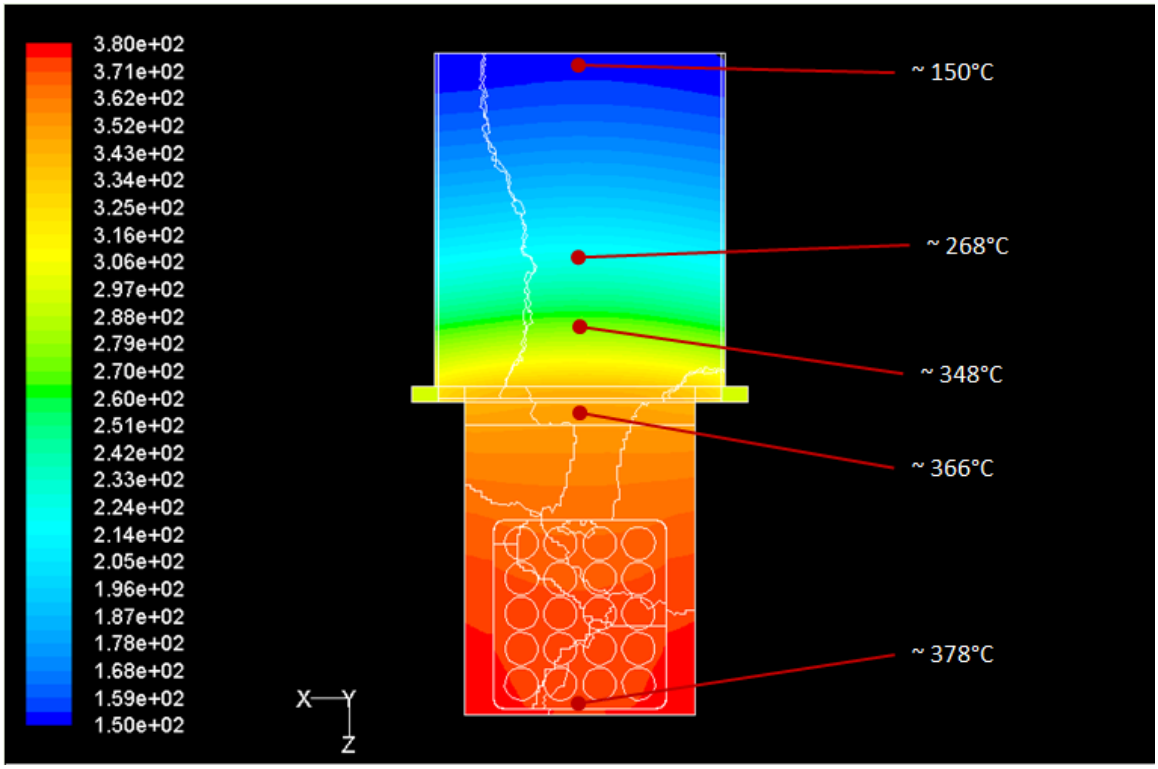

Figure 35: Results from the Detailed 3D Model. Shutter and Shutter Guide Only. Temperature in °C shown on left.

6.3 Evaluation of a method to Increase the Steady State Temperature of the Shutter.

One concept that could increase the steady state temperature of the shutter is to reduce the heat conducted through the shutter to the shutter guide. On paper this concept is very appealing and can be implemented with no modification to the shutter mounting or guide. This method was modeled to determine the effectiveness of the concept and as a tool to determine whether it should be implemented.

The results of the reduced conduction shutter concept can be seen side-by-side with a standard shutter in Figure 36. The reduced conduction shutter is predicted to increase the overall temperature of the shutter to 380-390°C. This increase is still below the temperature needed to stop condensation, and while the theory behind the concept proved correct, the overall effectiveness of the design is not enough to warrant the cost of implementation. This model will continue to be used to test other design concepts as the work to eliminate the chemical condensation into the shutter continues.

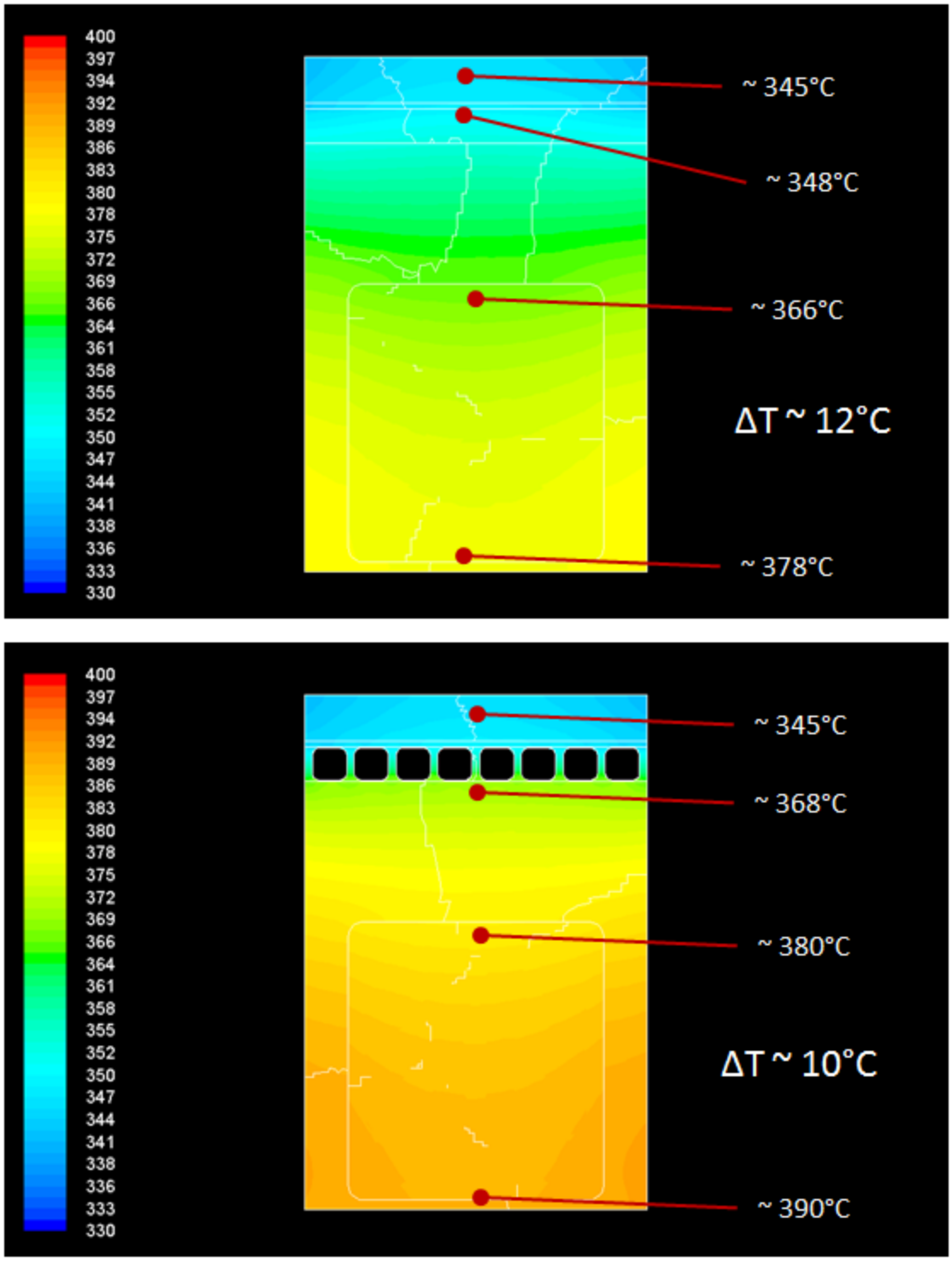

Figure 36: Results of Reduced Conduction Shutter (bottom) alongside a Standard Shutter (top). Temperature in °C shown on left.

6.4 Evaluation of the Shielding Approximation and Overall Thermal Uniformity of the Deposition Station.

Figure 37, 38, and 39 show comparisons between the detailed model run without shielding, with shielding and with the original emissivity shielding approximation. The no shielding model distinctively shows a lower temperature across both the top and bottom sources. Both the shielded and shielding approximation models show similar thermal patterns within the sources and almost identical thermal gradient pattern to the previous simple 3D station models. It can be seen that there is a slight difference in the thermal gradient patterns toward the surface of the sources in between the two shielding models; the results suggest that the difference is negligible for most design evaluations. It can be concluded that approximating the shielding by lowering the emissivity of the outer surface is a good method for first order evaluation of new design concepts.

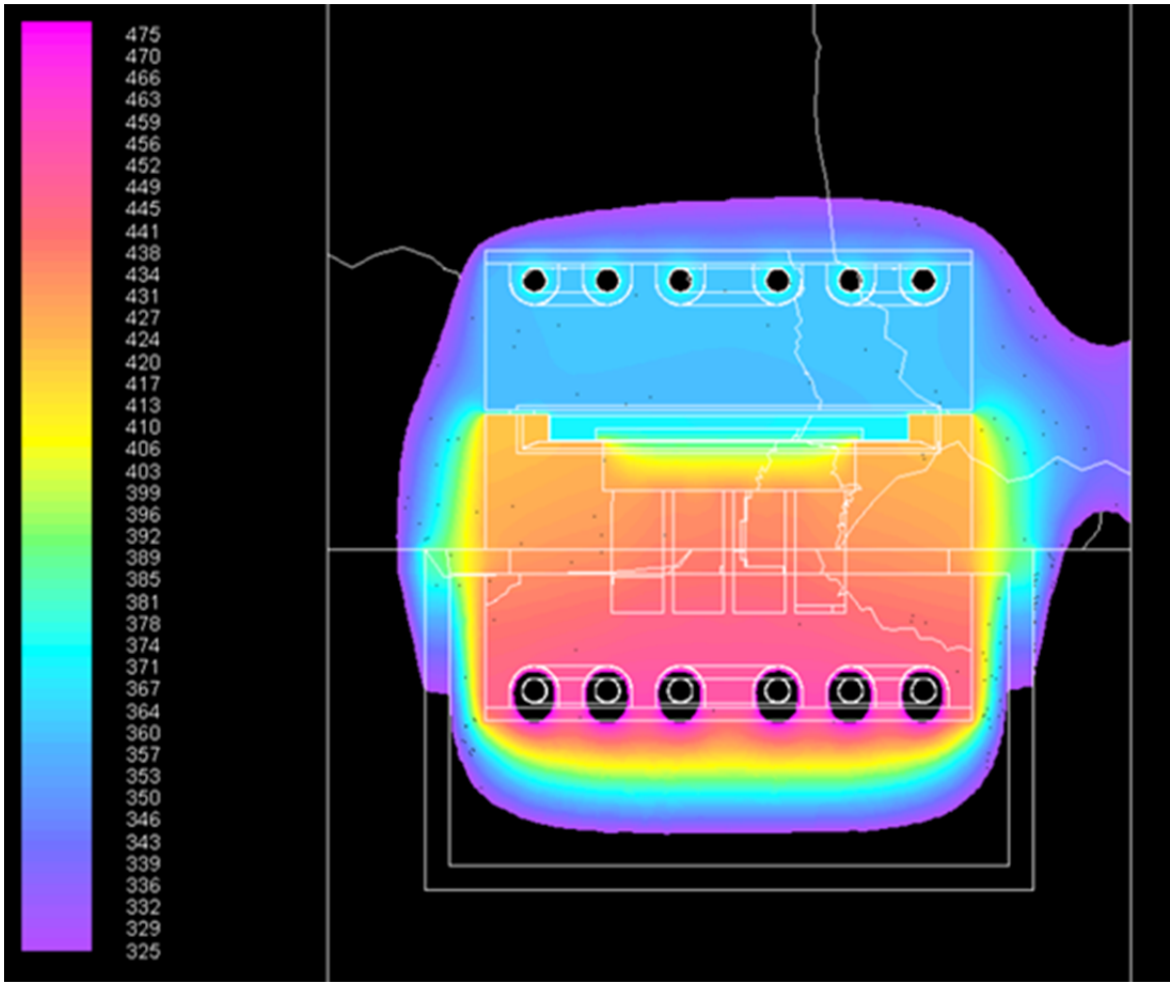

Figure 37: Detailed Model Run without Shielding. Temperature in °C shown on left.

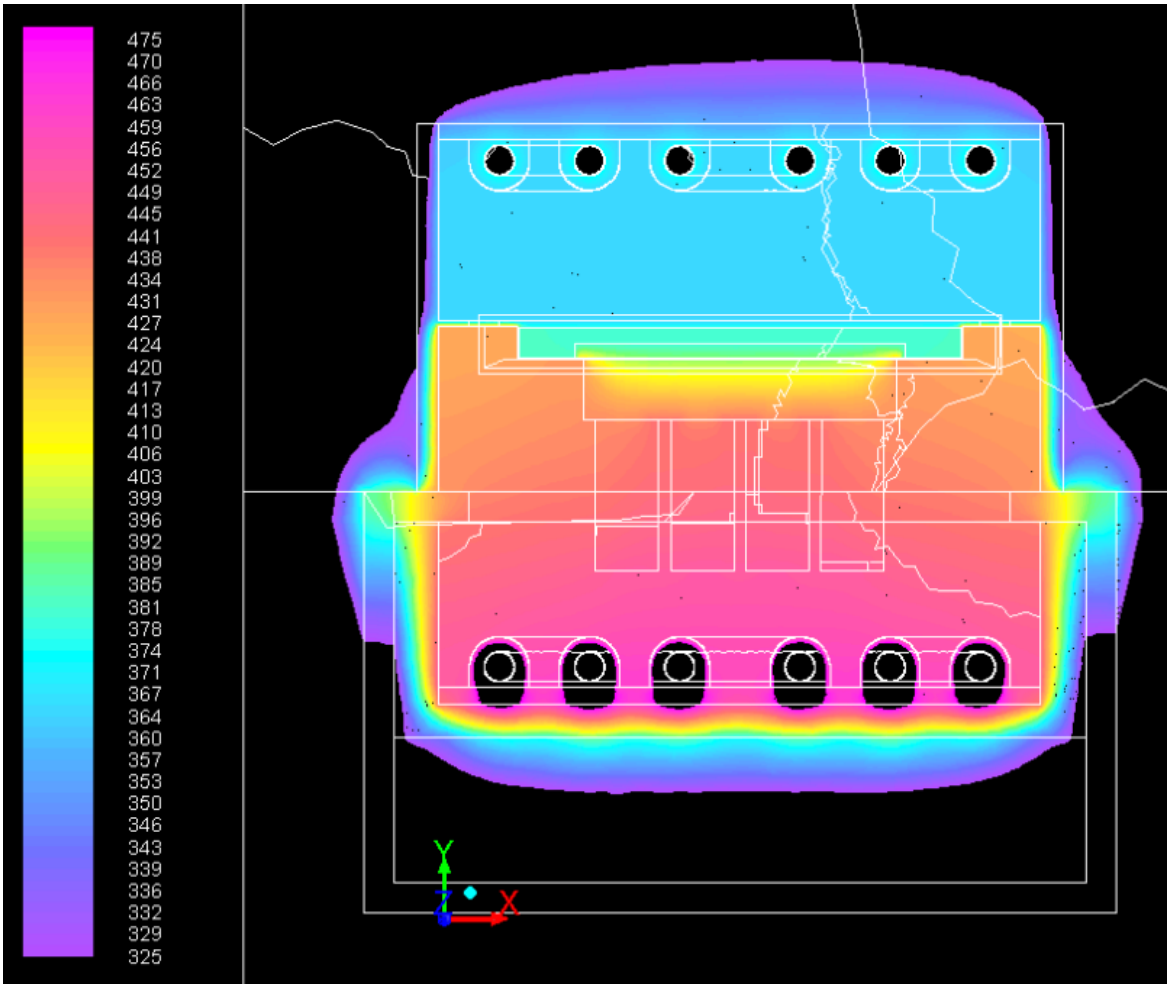

Figure 38: Detailed Model Run with Shielding. Temperature in °C shown on left.

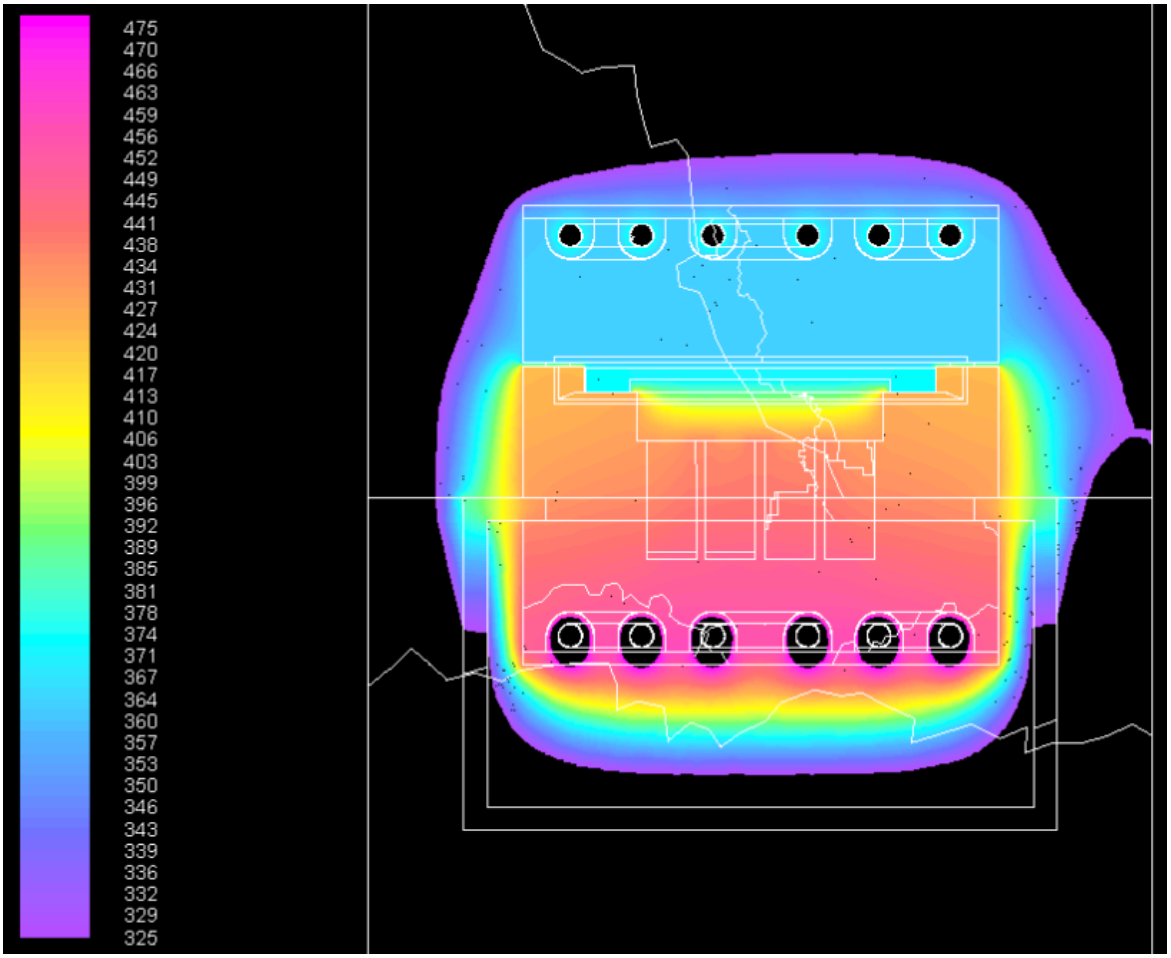

Figure 39: Detailed Model with Shielding Approximations. Temperature in °C shown on left.

Chapter 7: Modeling of Industrial Scale System.

7.1 Motivation.

As stated earlier, Abound solar was created from the materials engineering laboratory at Colorado State University. Abound solar is also an active part of the Industrial / University Cooperative Research Center with the Vice president of research is the chairman of the I/UCRC industrial advisory board. The engineering group at Abound solar became interested in the quality and in-depth level of model work done for the ARDS project. This resulted in a modeling effort with Abound Solar to optimize their manufacturing systems.

A focused project was started under the I/UCRC to begin modeling the Abound semiconductor manufacturing system. The project was broken up into three distinct tasks. The first task was to establish a base line model of the glass heating station in the original design of the semiconductor processing station (cell 1). The goal of the first task was to investigate the thermal gradients across the glass substrate created by this station. The second task involved modeling the new glass heating station to investigate the thermal uniformity of this newly developed station (cell 2). The third task was to begin modeling new design concepts in support of development of an improved top heating unit for the chemical stations.

Permission has been granted to publish the work done for task 1 and the results from task 2 in this thesis.

7.2 Glass Heating Station Modeling Project Overview.

The first station in the semiconductor deposition system is a glass heating station. This station heats the glass to the required temperature for deposition of the CdS layer. It is very important that the glass is heated uniformly in this station. Non-uniform heating can cause three major problems. First the glass used on industrial panel is tempered to meet safety standards. If the glass is held at high temperature for a long period of time it will begin to relax the internal stress essentially annealing the glass. This loss of temper can lead to breakage during the manufacturing process. Second, if the glass reaches temperatures above the softening point of approximately 525°C, permanent deformation can occur. Third, non-uniform temperature across the glass will cause uneven film growth leading to a loss in panel performance and efficiency.

The cell 1 design was creating some abnormalities around the edge of the panel. The focus of the task 1 project was to investigate the thermal gradients cause by the heating station to gain insight into areas to focus optimization efforts.

7.1 Cell 1 Model Design.

Previous modeling work had been done for the cell 1 heating station using ANSYS mechanical Finite element solver. It was determine to use the same model layout used in the mechanical models as a base line for the initial models in Fluent.

The model contains only what would be considered thermally critical parts. These parts included the heating elements, heat spreaders, upper heat spreader supporting rails,

glass substrate, belt support rails, and enclosure, see Figure 38. The enclosure has been segregated to create surfaces at the front and back that will be used as black body zones approximating the gap in the shielding for substrate motion.

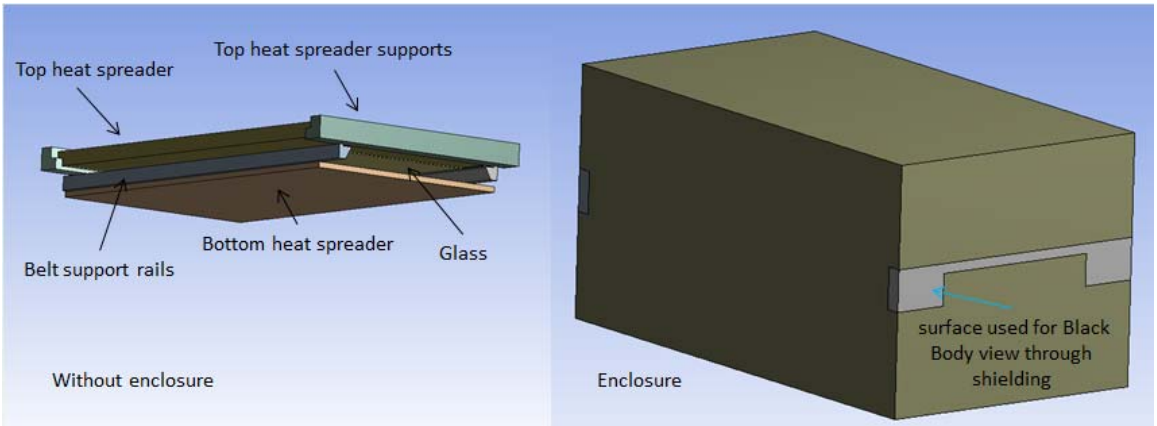

Figure 40: Cell 1 Model Layout.

Boundary conditions of the enclosure at the black body zones are set as either the load lock entrance temperature of 50°C or a CdS zone temperature approximation of 600°C. Both black body zones emit to a constant temperature emitter with an emissivity of 1.0. The remaining surfaces of the enclosure were called out as 4" thick insulation board emitting to a far field of 26°C with an external emissivity of 0.5 and an internal emissivity of 0.45.

These boundary conditions approximated the fiber board insulation and far field conditions surrounding the heating station. There are additional radiation shielding packs that are placed between the fiber board and the heating station components that are approximated by dropping the emissivity of the outer surfaces of the heat spreaders.

7.2 Belt to Glass interface approximation.

The glass is transported by a sheet metal belt. The interface between the glass and belt and the belt and belt support is a difficult structure to model in Fluent. It is assumed that the glass only contacts the belt at only a few points. This means the dominant heat transfer mechanism between the belt and glass is radiation. In order to model this arrangement it would require meshing a very thin nitrogen zone between the belt and the glass creating very small cells and resulting in an unmanageably large model. In addition to the thin radiation zone, the belt itself is only 0.018" thick also yielding to very small cells if meshed as part of the model. Again, the Fluent CFD solver allows a single surface to be given specific material properties and thickness which are used to calculate the heat transport across the surface. Essentially this technique produces a unique thermal resistance across the surface. To overcome the problem of having a thin radiation zone on top of a thin material, a set of pseudo material properties were developed to apply to the interface zone between the glass and the belt rails, eliminating the belt and thin radiation zone from the model. To do this, the material properties of the Inconel belt were used with the conductivity of the material modified to match the effective resistance across the radiation zone. To calculate the new conductivity the heat flux across the zone is assumed constant along with the temperature of both the glass and belt support rail.

This allows the equation for heat flux through the pseudo material (conduction) to be set equal to the radiation heat flux equation across a zone of similar thickness. The resulting equation is then solved for the new thermal conductivity as in Figure 39.

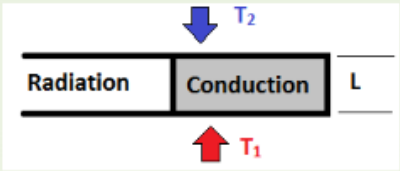

$$k = x\left[\frac{\sigma L\left(T_1^4 - T_2^4\right)}{\frac{1}{\epsilon_1}+\frac{1}{\epsilon_2}-1}\right] + (1-x)b$$

- k= Equivalent conductivity.
- x= % Radiation coupled.
- σ= Stefan-Boltzmann constant.
- L= Thickness of solid.
- T_1= Temperature of base.
- T_2= Temperature of part.
- ϵ_1= Emissivity of base.
- ϵ_2= Emissivity of part.
- b= Solid material conductivity (maximum conductivity if boundary is conduction only).

Figure 41: Equation Used for Belt Zone Approximation.

To verify that this approximation should produce accurate results around the belt to glass interface, 2D models were produce to test the theory, Figure 40. The results of the test can be seen in Figure 41 where the thermal gradient pattern in the model with the pseudo material. The thermal gradient patterns of the presumed match the assumed accurate case.

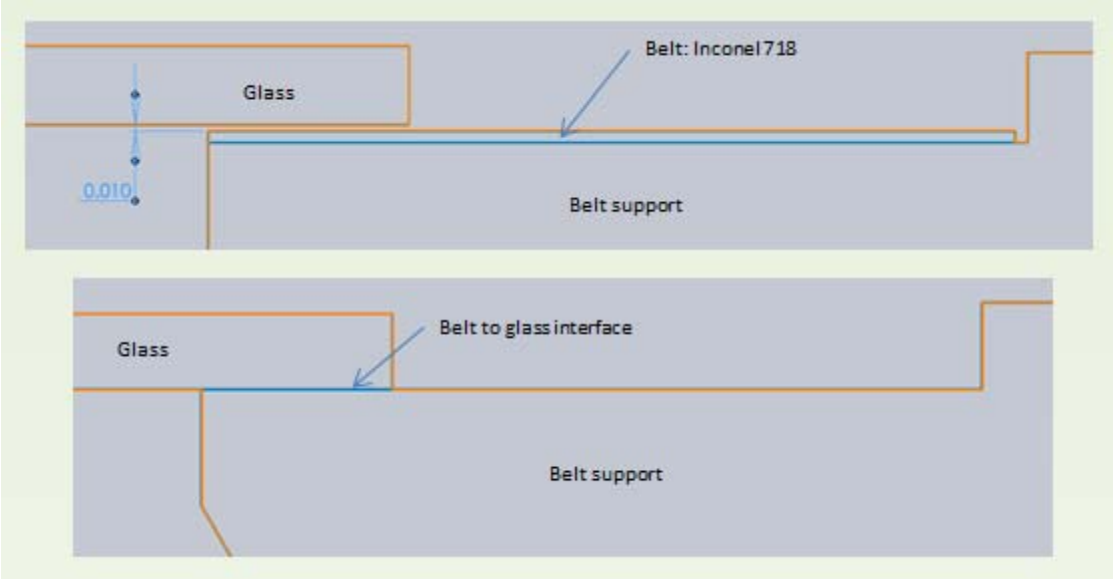

Figure 42: 2D Model Lay Out for Belt Approximation Test. Top Actual Zone. Bottom Approximation.

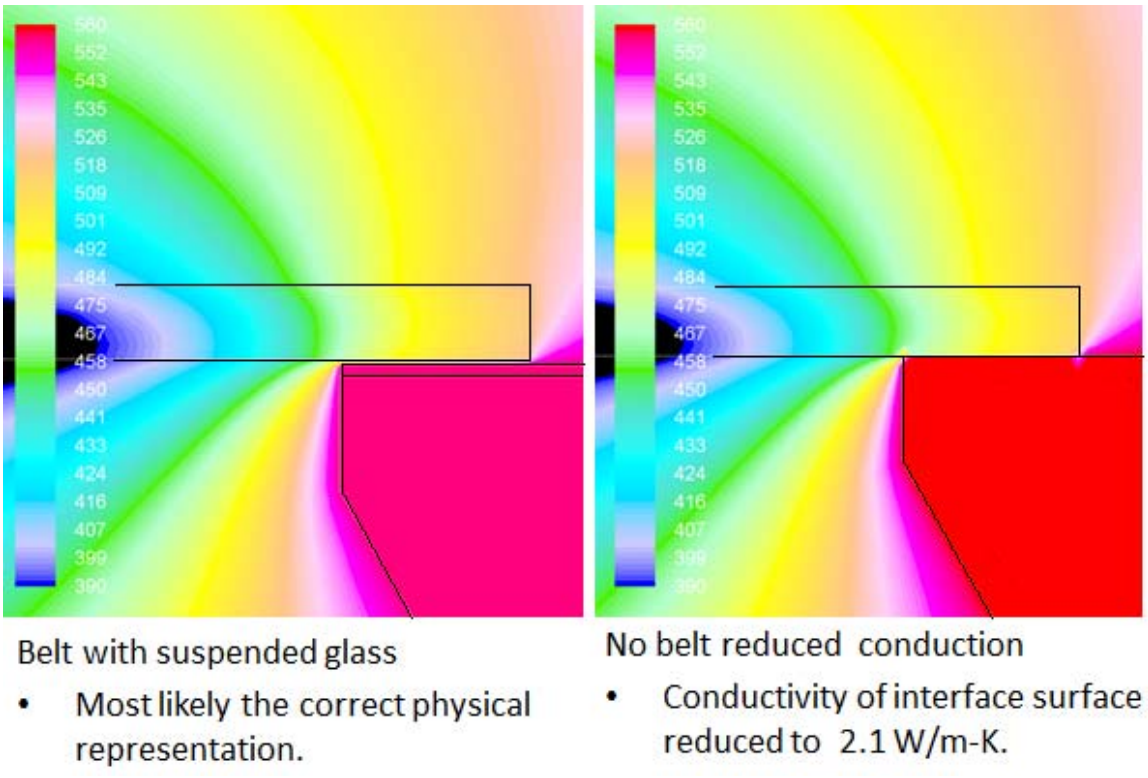

Figure 43: Results from 2D Belt Approximation Test. Temperature in °C shown on left.

7.3 Results from Cell 1 Model.

To gain accurate results, the model must be run as a transient calculation starting from a steady state conditions for the glass heaters. Temperature of the heat spreaders is measured at given positions. There is no direct monitoring of the heater element temperature in the production system. To produce the same effect in the model, the heaters are set at constant temperature and the heat spreader temperature is checked at the monitoring locations. The heater temperature is then modified until it produces a desired steady state temperature at the monitoring locations within the heat spreaders. Once the model matches the desired steady state conditions, the steady state solver is switched to a transient solve, the temperature of the glass is reassigned to 26°C to emulate a fresh incoming substrate, the model is then ran for the 120 sec time duration of the production system. To account for the heat loss to the glass during the 120 sec. cycle, the temperature of the heaters is increased at the beginning of the transient run. The temperature of the heat spreaders is then checked at the end of the 120 sec transient run and the amount of temperature increase to the heaters is change until the correct setting is found that will compensate for the heat loss to the glass without changing the temperature of the heat spreaders at their temperature monitoring locations.

The results of the model show that the uniformity across the bulk of the glass is with 10°C. The model also predicts a hotter zone around the perimeter of the glass with a hot zone over the belt, Figure 42. This effect is caused by the added absorption of radiation by the edges of the glass. Additionally, the hotter zones down the sides supported by the belt are created by the saturation of heat at the belt zone itself. From a close-up of the upper left corner of the glass we can see that this effect is creating a

thermal gradient of approximately 156°C over a short distance diagonally across the glass, Figure 43. It can also be seen that the very edge of the glass over the belt could be reaching temperature high enough to cause plastic deformation. The next analysis was performed on the cell 2 design.

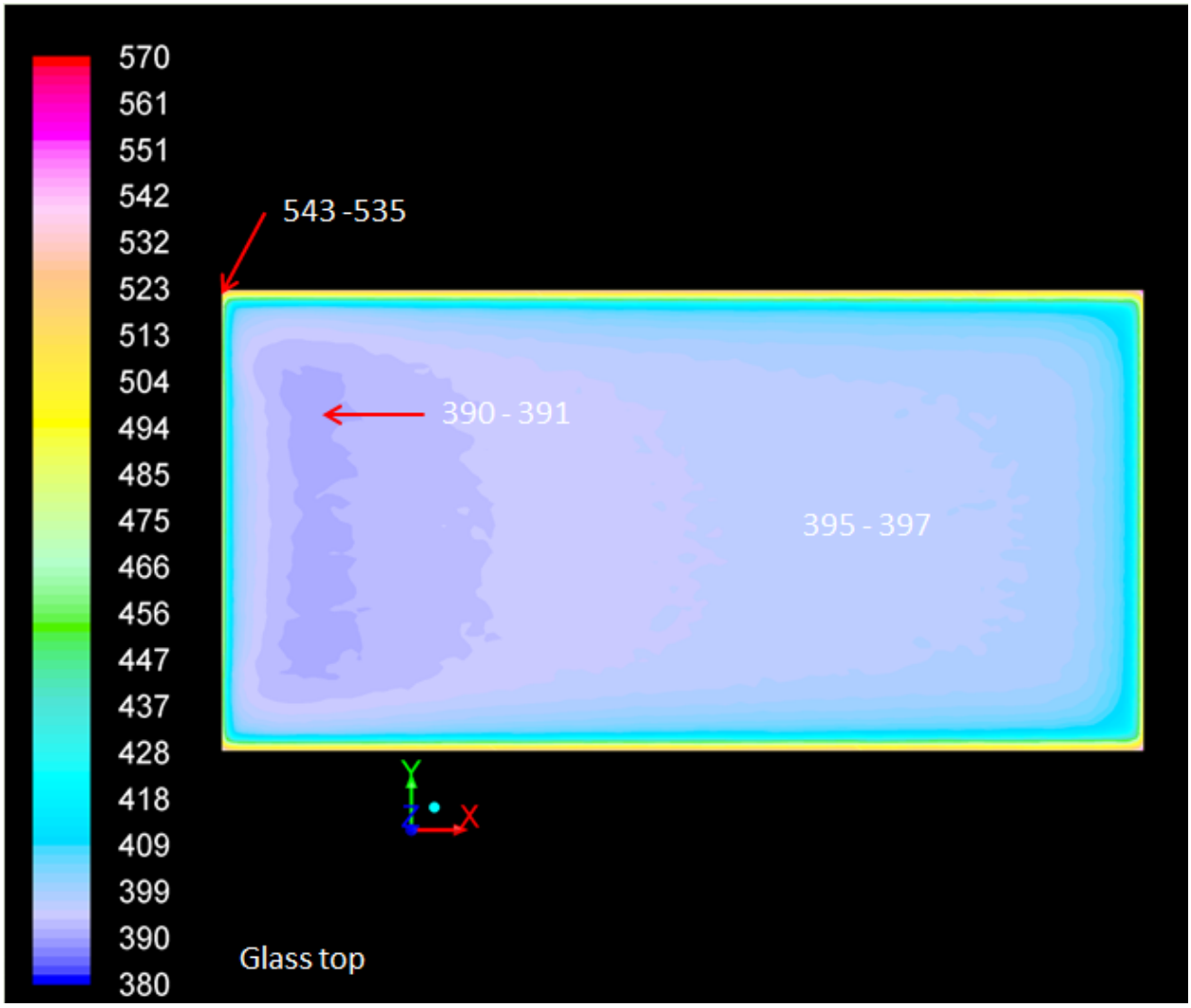

Figure 44: Image of the Glass from Cell 1 Model. Temperature in °C shown on left.

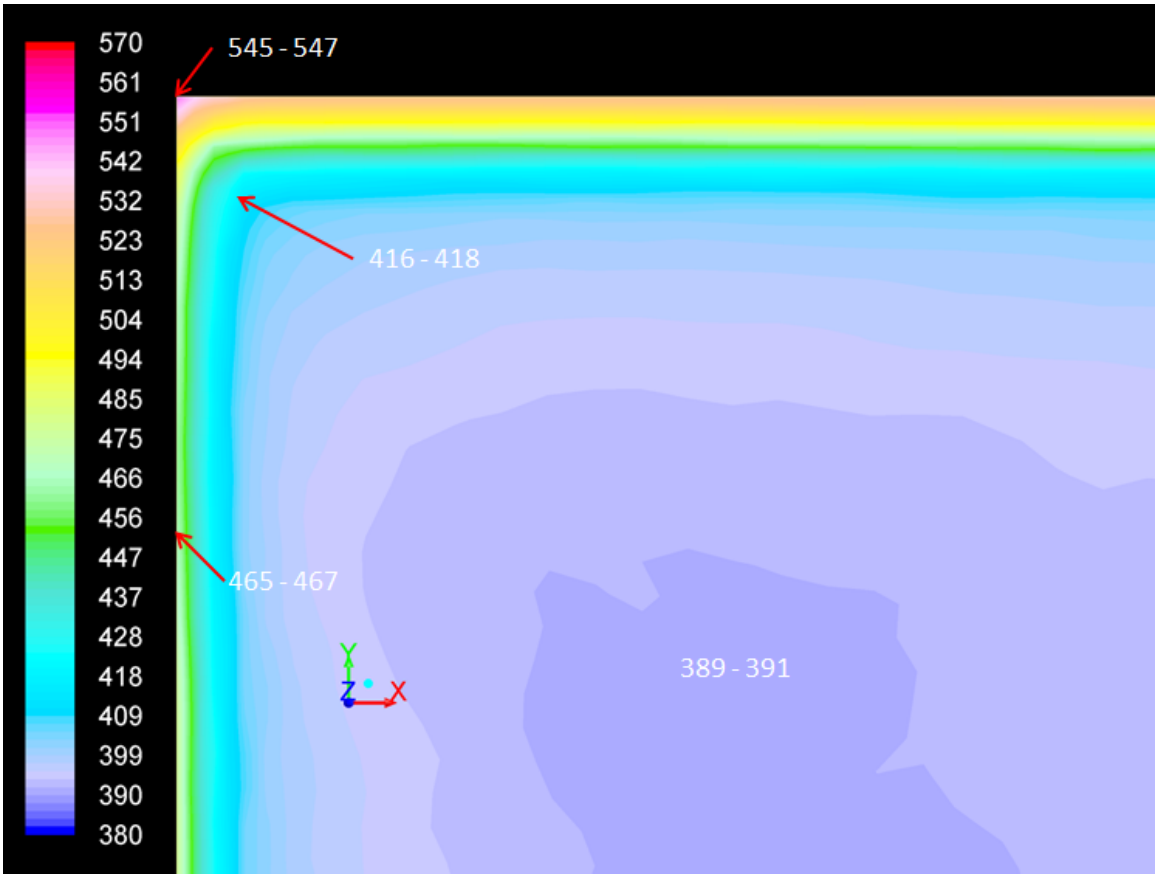

Figure 45: Close-up of the Upper Left Corner of the Glass: Cell 1 Model. Temperature in °C shown on left.

7.4 Cell 2 Heating Station Modeling.

Due to the quality and quantity of the data gained from the cell 1 modeling task, it was decided that the new cell 2 design should be modeled. The cell 2 design was in the later stages of assembly when this decision was made; being so, the opportunity to add additional testing to verify and calibrate the models was available. In addition to the opportunity to add additional temperature monitors to the system during initial start-up and testing of the new cell 2, the new system was designed to incorporate a scanning infrared camera to the interstitial zone between stations. This new scanning IR camera would give detailed thermal images of the glass as it moves out of the heating station and into the CdS deposition station. Throughout the modeling effort for the development of the ARDS at Colorado State University and the Modeling effort done for Abound Solar, there has not been good quality experimental data available to verify the accuracy of the model. The scanning IR camera brought the opportunity to verify the accuracy of the models, thus providing the confidence necessary to begin using them for design evaluation and performance prediction.

It was decided that the heating station for cell 2 should be modeled in detail. This would include modeling all of the internal shield packs as well as most of the internal support structures. This produced some of the largest models to date with the final model exceeding 27 million cells. In order to produce these large scale models Abound Solar supplied two large server computers and the ANSYS licensing necessary to efficiently create and run these models.

Due to the proprietary nature of the new design and contractual obligations between Colorado State University and Abound Solar, the geometry of the system cannot be presented. Permission has been granted to publish the results from the model compared to the data collected form the scanning IR camera.

7.5 Cell 2 Model Results.

The initial results from the model depict similar results obtained from the cell 1 modeling effort. When compared to the images of the scanning IR camera we can see that the model predictions are almost identical to the actual system, Figure 44.

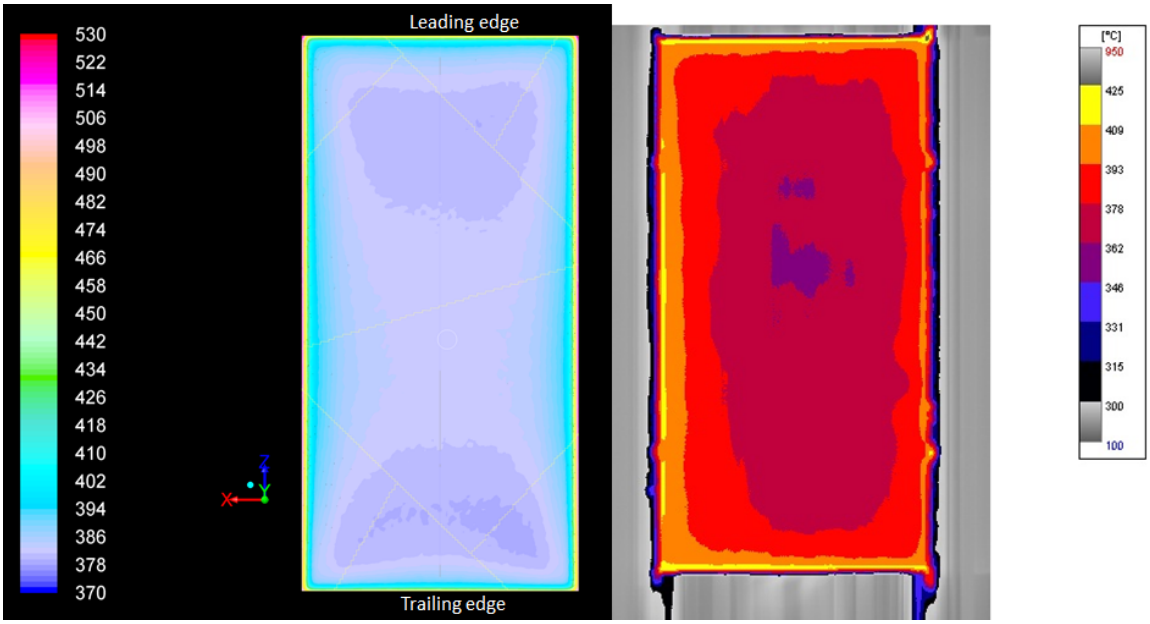

Figure 46: Cell 2 Model (left) vs. Scanning IR Camera Image (right). Temperature in °C shown on left and right sides

When the temperature profile, down the centerline of the glass is plotted form both the model and the IR camera, we see that the model and the measured data are within 10°C.

The model does predict the edge at a higher temperature than the scanning IR camera; however the model has a significantly high resolution. The average cell size along the edge of the glass in the model is approximately 1mm (0.039”).

The spot size of the IR camera is approximately 0.5” and the scan rate produces a data point at 0.125” intervals. These data points are then averaged together to create the image. When the data from the edge of model is averaged over a 0.5” the results are again within 10°C (± 2.5%) of the measured data, Figure 45.

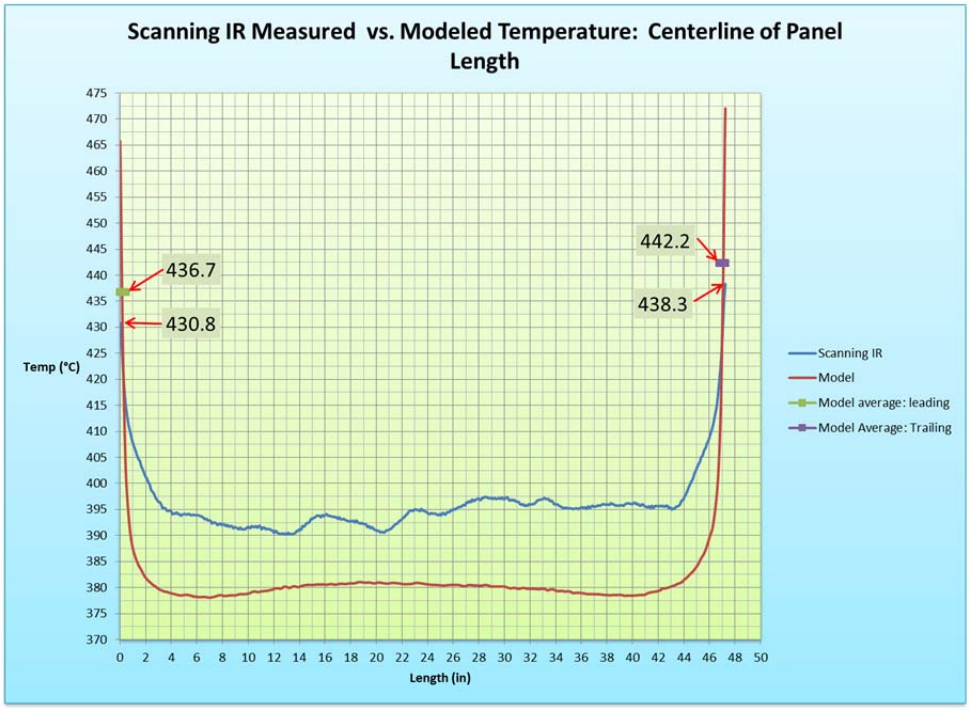

Figure 47: Temperature Comparison of Model to Scanning IR Camera. Down Centerline of Glass.

Chapter 8: Conclusions

8.1 Overall Modeling Conclusions.

From the modeling effort done for both the Materials Engineering Laboratory and from the work done for Abound Solar, computer model has been shown to be a valuable tool to be used for the design and development of photovoltaic manufacturing equipment. It gives the engineer the ability to investigate design performance in of processes within environments where it is difficult to perform accurate measurements. It can be used to create virtual prototypes and evaluate these designs before committing resources to the project, saving both time and money. It can also be used to optimize system parameters and find possible areas for improvement within the manufacturing system without interfering with the productivity and operation of the plant for testing.

8.2 Future work at Colorado State University.

The entire modeling effort to date has been focused on thermal modeling. The fluid flow solver within Fluent has not been used for any of the modeling effort. This means that to date only a small part of the modeling capabilities of Fluent have been investigated. Future work should include an investigation into chemical flow within the deposition pocket and the flow of chemicals that have escaped the deposition pocket. Any chemical that escapes the deposition pocket is considered a contaminant to the rest of the

system. Work to evaluate the flow patterns within the system and design changes that can be used to control and or contain contamination should be evaluated. Additionally work can be done to model the film growth process and species transport between the deposition pocket and the glass substrate.

8.3 Future work.

The cell 2 models have already been used to evaluate process parameters settings that have increased the thermal uniformity of the glass as it travels through the system. Work is continuing on the task three phase of the project to evaluate new design changes to the top heating units in an effort to boost both module efficiency and production system efficiency.

References:

1. Metz B, Davidson O, Bosch PR, Dave R, Meyer LA. Summary for policymakers. *Climate change*. 2007.

2. Administration UEI, (US) EIA. *Annual Energy Review, 2009*. Energy Information Administration; 2009.

3. Hadley SW, Tsvetkova AA. Annual Energy Outlook 2011, with Projections to 2035. *The Electricity Journal*. 2009;22(10):56–68.

4. Anon. key_stats_2010.pdf. Available at: http://www.iea.org/textbase/nppdf/free/2010/key_stats_2010.pdf. Accessed August 13, 2011.

5. (US) EIA. *Renewable Energy Consumption and Electricity Preliminary Statistics 2010*. Energy Information Administration; 2011.

6. Anon. Solar | Department of Energy. Available at: http://energy.gov/solar. Accessed September 10, 2011.

6. Brian, Davis. Energy & Evironment Consumer Survey. *Research Rport.* Pike Research, 1Q 2011.

8. Anon. EIA Renewable Energy-Solar Photovoltaic Cell/Module Manufacturing Activities. Available at: http://www.eia.gov/cneaf/solar.renewables/page/solarreport/solarpv.html. Accessed August 28, 2011.

9. Selya Price, Robert Margolis. 2008 SOLAR TECHNOLOGIES MARKET REPORT. 2010.

10. Department of Energy. SunShot Initiative: About. Available at: http://www1.eere.energy.gov/solar/sunshot/about.html#background. Accessed August 13, 2011.

9. *Greentech Media Research.* http://www.gtmresearch.com/

10. *Lux Research Inc*. http://www.luxresearchinc.com/coverage-areas/solarsystems.html.

13. Alsema EA, de Wild-Scholten MJ, Fthenakis VM. Environmental impacts of PV electricity generation-a critical comparison of energy supply options. In: *21st European photovoltaic solar energy conference, Dresden, Germany*.Vol 3201.; 2006.

14. W.S. Sampath, K.L. Barth, R.A. Enzenroth. Advances in Continuous, in-lineprocessing of stable CdS/CdTe devices. Available at: http://ieeexplore.ieee.org/stamp/stamp.jsp?arnumber=01190624. Accessed September 10, 2011.

15. Anon. July09_Hydrocarbon_Article.pdf. Available at: http://www.callidus.com/Documents/July09_Hydrocarbon_Article.pdf. Accessed August 13, 2011.

15. National Science Foundation Bule Ribbon Pannel on Simulation-Based Engineering Science. *Simulation-Based Engineering Science,* sbes_final_report.pdf. National Science Foundation, May 2006.

16. Anon. ANSYS Fluent Theory Guide. ANSYS Inc. Release 13.0, November 2010

Appendix

A1: General

Solver:

- Pressure based.
- Absolute velocity formulation.
- Steady State or Transient depending on simulation type.
- No gravity.

A2: Models

- Multiphase – off
- Energy – on
- Viscous – Laminar
- Radiation – Discrete ordinate (DO)
    - DO/Energy coupling – off
    - Solar load – off
    - Flow iterations per radiation iteration – 1
    - Theta divisions – 2
    - Phi divisions – 2
    - Theta pixels – 1
    - Phi pixels – 1
    - Number of gray bands – 0
- Heat exchanger – off
- Species – off

- Discrete phase – off
- Solidification & melting – off
- Acoustics – off

A3 Materials

The main working fluid is typically nitrogen using the ideal gas law for density. Kinetic theory is used for specific heat, thermal conductivity, and viscosity. All other properties are left at their default value.

A4 Cell zone conditions

Only the fluid zones participate in radiation. The operating condition is set at 5.33Pa with no gravity.

A5 Boundary conditions

Outer enclosure surfaces will be set as radiation:

- External emissivity – 0.7
- External temperature – 26°C
- Internal emissivity – this will vary depending on assumptions of model.

The enclosure may or may not be given a material designation and thickness. This will depend on model assumptions.

Inner radiating surfaces will be set with the emissivity of the material they represent.

Inner shielding surfaces will be set with the appropriate emissivity, material designation, and thickness.

Heater surfaces will be given either a constant temperature or a constant heat flux depending on model assumptions.

A6 Solution Methods

Pressure velocity coupling:

- Scheme – Simple

Spatial discretization:

- Gradient – least squares cell based
- Pressure – second order
- Density – second order upwind
- Momentum - second order upwind
- Energy - second order upwind
- Discrete ordinate - second order upwind
- Transient formulation – second order implicit (when used)

A7 Solution Controls

All solution controls are left at default values. Under equations, the flow equations are turned off.

A8 Monitors

The convergence criterion for the energy equation is left at the default value of 1e-6.

The convergence criterion for the DO equation is decreased to 1e-5.

Additional temperature monitors should be used for steady state calculations. These monitors should be created using point surfaces at the locations where the control thermocouples are in the source being evaluated. Their output should be set as the area weighted average of temperature and printed to console so they can be monitored by the operator.

A9 Run Calculation

Steady state calculations are ran at default run calculation settings until convergence is reached or temperature monitors show steady state condition has been reached.

Transient calculations should use 1 sec/ time step interval with the maximum number of iterations per time step increased to 100 to assure convergence during the first time steps.